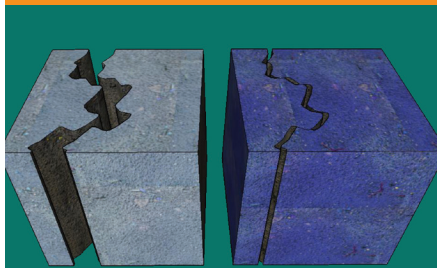


Original Research



Soil fissures and small cracks develop as a result of matrix shrinkage; upon wetting, the soil matrix volume increases by swelling, thereby partially closing the cracks and fissures. We propose a model for flow and transport accounting for the geometrical deformation of both the soil matrix and the fracture porous systems, as well as for the dynamics of hydraulic properties in response to the domain deformations.

Antonio Coppola and Alessandro Comegna, School of Agricultural, Forestry, Food and Environmental Sciences (SAFE), Hydraulics Division, University of Basilicata, Potenza, Italy; Giovanna Dragonetti, Mediterranean Agronomic Institute, Land and Water Division, IAMB, Bari, Italy; Horst H. Gerke, Inst. of Soil Landscape Research, Leibniz-Centre for Agricultural Landscape Research (ZALF), Müncheberg, Germany; Angelo Basile, Inst. for Mediterranean Agricultural and Forestry Systems (ISAFoM), National Research Council (CNR), Ercolano (Napoli), Italy. *Corresponding author (antonio.coppola@unibas.it).

Vadose Zone J.
doi:10.2136/vzj2015.02.0021
Received 4 Feb. 2015.
Accepted 17 June 2015.

© Soil Science Society of America
5585 Guilford Rd., Madison, WI 53711 USA.
All rights reserved.

Simulated Preferential Water Flow and Solute Transport in Shrinking Soils

Antonio Coppola,* Alessandro Comegna, Giovanna Dragonetti, Horst H. Gerke, and Angelo Basile

We present follow-up work to previous work extending the classical rigid (RGD) approach formerly proposed by Gerke and van Genuchten, to account for shrinking effects (SHR) in modeling water flow and solute transport in dual-permeability porous media. In this study we considered three SHR scenarios, assuming that aggregate shrinkage may change either: (i) the hydraulic properties of the two pore domains, (ii) their relative fractions, or (iii) both hydraulic properties and fractions of the two domains. The objective was to compare simulation results obtained under the RGD and the SHR assumptions to illustrate the impact of matrix volume changes on water storage, water fluxes, and solute concentrations during an infiltration process bringing an initially dry soil to saturation and a drainage process starting from an initially saturated soil. For an infiltration process, the simulated wetting front and the solute concentration propagation velocity, as well as the water fluxes and water and solute exchange rates, for the three SHR scenarios significantly deviated from the RGD. By contrast, relatively similar water content profiles evolved under all scenarios during drying. Overall, compared to the RGD approach, the effect of changing the hydraulic properties and the weight of the two domains according to the shrinkage behavior of the soil aggregates induced a much more rapid response in terms of water fluxes and solute travel times, as well as a larger and deeper water and solute transfer from the fractures to the matrix during wetting processes.

Abbreviations: RGD, rigid hypothesis; SHR, shrinking hypothesis; TDR, time domain reflectometry; VG, van Genuchten hydraulic functions.

Preferential flow paths are naturally present in soils as a result of the complex interactions among soil microstructure, water, solutes, and soil biota activities, which frequently induce a partition of the soil pore system into two or more separate porous systems characterized by different water flux densities and interconnected to different extents. The velocity of water in the preferential flow paths may be even several orders of magnitudes larger than in the surrounding less permeable matrix. As a consequence, preferential flow may induce local scale nonequilibrium conditions in pressure head and solute concentrations between regions of faster and slower flow (Beven and Germann, 1982; Gerke and van Genuchten, 1993a; Jarvis, 2007; Coppola et al., 2009a,b). Water and solutes infiltrating in the soil do not equilibrate with the resident soil water pressures and solute concentrations, thus flowing rapidly to deeper soil horizons and groundwater. This has obvious effects on water and solute storage along the soil profile, which in turn condition water and solute uptake by plant roots and evaporation from the soil surface.

A two-domain approach to account for a faster and a slower transport region is generally applied (e.g., Germann and Beven, 1985; Gerke and van Genuchten, 1993a; Greco, 2002; Larsbo and Jarvis, 2003; Jarvis, 1994). Several applications of the model to flow and transport in structured soil proposed by Gerke and van Genuchten (1993a) use Richards' equation for both pore domains (e.g., Gerke and Köhne, 2004; Ray et al., 2004; Dušek et al., 2006).

The model has been developed on the assumption of rigid porous media where preferential flow and slow flow domains are assumed to keep constant pore volume and pore-size distribution (i.e., only permanent fissures and fractures are present). This assumption was adopted in many of the dual-permeability approaches for describing flow and transport in soils with a network of preferential flow paths under nonequilibrium conditions (fast flow paths bypassing the surrounding matrix) (e.g., Hoogmoed and Bouma, 1980; Beven and Germann, 1982; Germann and Beven, 1985; Steenhuis et al., 1990; Wallach et al., 1998; Gerke and van Genuchten, 1993a; Emerman, 1995).

However, the pore systems in most natural soils are dynamically changing due to alternating swelling and shrinkage processes, which induces changes in pore volume and pore-size distribution including deformations in pore geometry (e.g., Richards and Peth, 2009; Horn, 2004). Significant pore-volume changes may be observed in both inorganic and organic soils (Peng and Horn, 2007) and are enhanced by expansive clay minerals (Tuller and Or, 2003.).

Subsidence, soil fissures, and small cracks generally develop as a result of matrix shrinkage. On wetting, the soil matrix increases its volume by swelling, thereby partially closing the cracks and fissures. Consequently, the flow and transport properties in the fast and slow flow domains are also dynamically changing with the geometrical properties of the porous medium. This is a serious difficulty for modeling flow and transport, as it will also require that the geometrical deformation of both the soil matrix and the fracture porous systems be taken into account, as well as the dynamics of soil hydraulic properties in response to the domain deformations.

Recently, Coppola et al. (2012) proposed an approach to account for the swell–shrink dynamics (SHR) in the classical (RGD) dual-permeability model of Gerke and van Genuchten. Conceptually, the soil in the SHR model was still treated as a dual-permeability bulk porous medium consisting of two dynamic interacting pore domains: (i) the fracture (from shrinkage) pore domain and (ii) the aggregate (interparticles plus structural pores), respectively (a porous systems classification suggested also by Abou Najm et al., 2010). In this classification, the aggregate domain coincides with what is generally called the soil matrix. This is why the terms *matrix* and *aggregate* domain will hereafter be used synonymously. In the approach of Coppola et al. (2012) the swell–shrink dynamics were represented by the inversely proportional volume changes in the fracture and matrix domains, while the overall porosity of the bulk soil, and hence the layer thickness, remained constant. In other words, the model assumed that the swell–shrink behavior of soil aggregates was accommodated within a crack network such that subsidence became negligibly small, with the result that the overall porosity related to the total (i.e., bulk) soil volume could be assumed constant (Bruand et al., 2001).

Hereafter, the abbreviations RGD and SHR will be used to identify, respectively, the approach assuming the rigidity of the porous

medium (RGD), as originally proposed by Gerke and van Genuchten (1993a), and the approach changing dynamically the relative contributions of the matrix and the fracture domains (SHR) according to the shrinkage characteristics of the matrix, as proposed by Coppola et al. (2012).

The RGD and SHR approaches are not complementary: the SHR approach does not aim simply to provide an additional mechanism to close the fractures of a porous medium already characterized by the RGD approach. On the contrary, they are alternative ways to characterize a dual-permeability porous medium hydraulically and to describe hydrological processes through that porous medium. If, for example, the evolution of the bulk water content was monitored at a control depth during a drying process, one could assume that the physical and the hydraulic characteristics of the two domains remained either constant (the RGD scenario) or changed during the drying (the SHR scenario). The problem is that, as discussed by Coppola et al. (2012), the relative contribution of the two domains to the same observed bulk water content will be different depending on the actual scenario (RGD or SHR). This may have important hydrological implications, as under the two scenarios the water (and solute) fluxes involved may be completely different. However, the dynamically changing domain-related fluxes and concentrations can hardly be measured directly such that these relative contributions need to be estimated using the proper model approach. In this sense, it is thus crucial to analyze the water flow and solute transport behavior in a wide range of water contents, from saturation to drier conditions, under scenarios RGD and SHR, by also considering the impact of drying and wetting processes. Accordingly, in this paper we compare the simulation results obtained under the RGD and SHR assumptions to illustrate the impact of matrix volume changes on water storage, water fluxes, and solute concentrations during: (i) an infiltration process bringing an initially dry soil to saturation and (ii) a drainage process starting from an initially saturated soil. Even if simulations were based on measured bulk and single-domain properties, we could not compare them to any measured fluxes dataset. In this sense, the work is a model sensitivity study mostly focused on evaluating the water flow and solute transport behavior under the different RGD and SHR scenarios.

The SHR approach originally proposed by Coppola et al. (2012) assumed that the aggregate shrinkage induced both a dynamic change in the hydraulic properties of the two domains and a dynamic change of the relative contribution (the weight) of the two domains to the hydrological behavior of the bulk soil. In this paper, we will introduce two “lighter” additional SHR approaches, where the aggregate shrinkage only induces either a change in the hydraulic properties or a change in weight.

Theory

Dual-Permeability Model for Soil Water Flow and Solute Transport

A dual-permeability bulk soil is generally assumed to consist of two dynamic interacting pore domains: (i) the fractures (from shrinkage) pore domain and (ii) the aggregates (matrix) pore domain. The two domains are characterized by specific hydraulic properties. In the Gerke and van Genuchten model, two coupled Richards' equations may be used to describe the transient water flow in the two domains. Similarly, solute transport in the two domains is governed by two coupled advection–dispersion equations. Details are given in the Appendix.

Porosities and Weight under RGD and SHR Assumptions

In general, Eq. [A1] and [A5] in the Appendix require that the water retention, $\theta(h)$, and hydraulic conductivity, $K(h)$, functions be known for both the domains, as well as the relative volumetric proportion of the fracture and aggregate pore system, β_f and $(1 - \beta_f)$, respectively.

The hydraulic properties and the weight will differ depending on the approach adopted (RGD or SHR).

Rigid (RGD)

The dual-permeability approach proposed by Gerke and van Genuchten (1993a) is based on the assumption that the properties of the bulk porous medium (subscript b) are given by the weighted contribution of the properties of each single domain as follows:

$$\varphi_b = \beta_{fR} \varphi_f + (1 - \beta_{fR}) \varphi_a \quad [1a]$$

$$\theta_b = \beta_{fR} \theta_f + (1 - \beta_{fR}) \theta_a \quad [1b]$$

$$q_b = \beta_{fR} q_f + (1 - \beta_{fR}) q_a \quad [1c]$$

where φ is the porosity, θ is the volumetric water content (i.e., the water volume, V_w , versus the total soil volume of the domain, V), and q is the Darcian flux density ($L T^{-1}$). As stated above, the weight β_{fR} (subscript R for rigid) is the fraction of total soil occupied by the fracture pore-system and may be expressed as a function of the porosities as:

$$\beta_{fR} = \frac{\varphi_b - \varphi_a}{\varphi_f - \varphi_a} \quad [2]$$

with $\varphi = e/(1 + e)$ being the porosity and e the void ratio, that is the ratio of V_p , the soil pore volume (subscript p), to V_m , the solid volume (subscript m). In a rigid soil with permanent preferential paths, both e_a (the void ratio for the aggregates) and e_f (the void

ratio for the fractures), and hence β_{fR} , do not depend on the water content or the pressure head.

Dynamic (SHR)

In the one-dimensional vertical model proposed by Coppola et al. (2012), aggregate deformation during wetting–drying cycles is assumed to change only the relative proportions of voids in the fractures and in the aggregates, while the total volume of pores (and thus the layer thickness) remains unchanged.

In other words, the partial contributions of the fracture and aggregate domains to the bulk porosity, $\beta_f \varphi_f$ and $(1 - \beta_f) \varphi_a$, respectively, are now a function of the water content (or the pressure head h), while their sum, the bulk porosity, φ_b , is assumed to be constant.

Characterizing matrix volume changes during drying–wetting cycles is based on the determination of the relationship between void ratio, e_a , pressure head, h , and moisture ratio, ϑ_a , of the aggregate domain (Bronswijk, 1991; Groenevelt and Grant, 2001, among others). The moisture ratio is defined as the ratio of soil water volume $V_{w,a}$ to the solid volume $V_{m,a}$ of the aggregate domain.

The shrinkage curve may be obtained by plotting e_a against the pressure head values h_a , and/or by plotting the void ratio e_a against the moisture ratio ϑ_a . The two curves may be simultaneously measured on undisturbed soil samples according to the procedure adopted by Garnier et al. (1997) and Coppola et al. (2012).

We refer the reader to the huge and exhaustive literature mainly devoted to discussing the physical significance of the different stages which can be identified along a shrinkage curve (see among others Bronswijk, 1991; Braudeau et al., 1999; Peng and Horn, 2005; Chertkov, 2007a,b; 2008). Details on the parametric functions for the shrinkage curves used for the numerical applications performed in this paper are given in the Appendix.

Once $e_a(h)$ is known, any change in the aggregate contribution to total porosity may be immediately converted into a proportional change in the fracture contribution to the bulk porosity. This condition may be fulfilled by considering three alternative approaches:

1. By allowing φ_a (and thus φ_f) to vary according to the $e_a(h)$ function and keeping the weight β_f constant to a value β_{fk} (subscript k for constant) (hereafter we will refer to this condition as SHR β_k).

$$\varphi_b = \beta_{fk} \varphi_f(h) + (1 - \beta_{fk}) \varphi_a(h) \quad [3a]$$

with β_f constant, the fractional contribution of the two domains to the bulk porosity may be immediately solved for each pressure head value from simple calculations involving the $e_a(h)$ relationship.

$$\varphi_a(h) = \frac{e_a(h)}{1 + e_a(h)} \quad [3b]$$

$$\varphi_f(h) = \frac{\varphi_b - (1 - \beta_{fk})\varphi_a(h)}{\beta_{fk}} \quad [3c]$$

$$\varphi_a(0) = \frac{e_a(0)}{1 + e_a(0)} \quad \phi_f(0) = \frac{\varphi_b - (1 - \beta_{fk})\varphi_a(0)}{\beta_{fk}} \quad [3d]$$

2. By fixing the aggregate and fracture porosity and allowing the weight $\beta_f(h)$ to change with h according to the $e_a(h)$ relationship. Hereafter we will refer to this condition as SHR $\beta(h)$.

$$\varphi_b = \beta_f(h)\varphi_{fk} + [1 - \beta_f(h)]\varphi_{ak} \quad [4a]$$

In this case, to deduce the shape of $\beta_f(h)$ from the $e_a(h)$ relationship we make the following assumptions:

- The porosity of the aggregate domain is set at the value at $h = 0$

$$\varphi_{ak} = \phi_a(0) = \frac{e_a(0)}{1 + e_a(0)} \quad [4b]$$

- At a given pressure head h , the fractional contribution of the aggregate domain to the bulk porosity in the SHR $\beta(h)$ case is set at the same value as in the SHR β_k case

$$[1 - \beta_f(h)]\varphi_{ak} = (1 - \beta_{fk})\varphi_a(h) \quad [4c]$$

In other words, the change in matrix porosity due to changes in water content is assumed to produce the same result on the aggregate contribution to the bulk porosity of a change in the weight of the aggregate pore system.

Consequently,

$$\beta_f(h) = 1 - \frac{\varphi_a(h)}{\varphi_{ak}}(1 - \beta_{fk}) \quad [4d]$$

which means that $\beta(h) = \beta_{fk}$ at $h = 0$ such that φ_{fk} is still the $\varphi_f(0)$ obtained in SHR β_k , just as for the aggregate domain

$$\varphi_{fk} = \varphi_f(0) = \frac{\varphi_b - (1 - \beta_{fk})\varphi_a(0)}{\beta_{fk}} \quad [4e]$$

With this approach $\beta(h)$ takes approximately the shape of an exponential function.

3. By changing partly φ_a (and hence φ_f) and partly the weight β_f with h (the only SHR approach formerly adopted by Coppola et al. (2012):

$$\varphi_b = \beta_f(h)\varphi_f(h) + [1 - \beta_f(h)]\varphi_a(h) \quad [5a]$$

Hereafter we will refer to this scenario as the combination approach, SHRcomb, as it combines characteristics of cases SHR β_k and SHR $\beta(h)$.

As discussed by Coppola et al. (2012), in this case one has to guess a priori a possible shape of $\beta_f(h)$. Moreover, this may represent a serious limit to identify the parameters for $\varphi_f(h)$ and $\beta_f(h)$, which are highly correlated and thus their estimation may suffer from lack of uniqueness. In any case, these problems may mostly be solved by assuming an exponential shape of the type $\beta(h) = \beta_0 \exp(\kappa h)$, as suggested from the SHR $\beta(h)$ assumptions and identifying a critical pressure head, h_c , at which the shrinkage process is completed (when the void ratio is $e_a(h_c) = e_p$). This information may be drawn by the experimental shrinkage curves, calculating a maximum value, $\beta(h_c)$, for the weight by imposing the constraint

$$\max[\beta_0 \exp(\kappa h)] = \beta_0 \exp(\kappa h_c) = 1 - \frac{\varphi_a(h_c)}{\varphi_{ak}}(1 - \beta_{fk}) \quad [6]$$

The term on the right side of the equation represents the value calculated in the SHR $\beta(h)$ scenario for $h = h_c$. In other words, it is assumed that the weight in the combination approach cannot be larger than the weight in the SHR $\beta(h)$ approach calculated at the minimum void ratio, e_p , assuming a nondecreasing $\varphi_f(h)$ function, $d\varphi_f/dh \geq 0$.

Figure 1 shows the extreme states of a shrinking–swelling soil volume. Starting from a completely saturated soil, the main consequence of aggregate drying is an increase in fracture porosity and a proportional decrease in aggregate porosity, thereby changing the ratio between the hydraulic properties of domains. The $e_a(h)$ curve will determine the rate of aggregate (and fracture) domain porosity changes with water contents. This rate will change in the different stages of the shrinkage curve. In our model the transition between the two extreme states evolves through changes in the porosities $\varphi_a(h)$ and $\varphi_f(h)$, the weight $\beta(h)$, or both in SHR β_k , SHR $\beta(h)$, and SHRcomb, respectively.

Hydraulic Properties in the Dual-Domain under RGD and SHR Scenarios

Within the RGD and SHR approaches, the water retention of the aggregate and fracture domains, as well as of the bulk soil, may be written in a general form relating the water content, moisture ratio and porosity of each domain as follows:

RGD

Aggregate domain

$$\theta_a(h) = \vartheta_a(h)[1 - \varphi_a(0)] \quad \varphi_a(0) = \frac{e_{a0}}{1 + e_{a0}} \quad [7a]$$

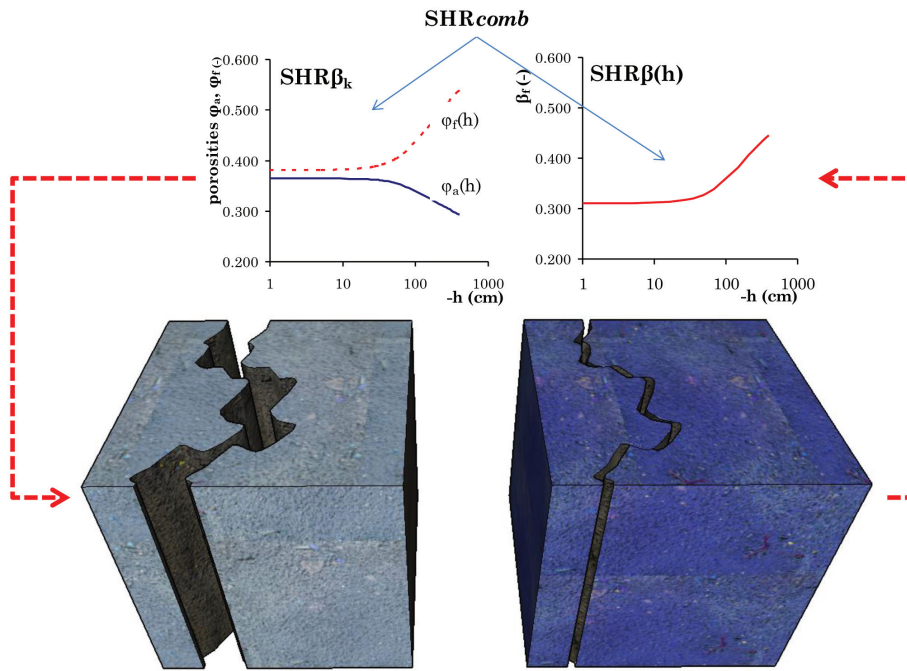


Fig. 1. Illustration of the model concept. The transition from the shrinkage state (left) and the swelling state (right) of the same volume evolves according to either the fracture and the matrix domain porosity changes ($SHR\beta_k$) or the $\beta(h)$ curve ($SHR\beta(h)$), or both ($SHRcomb$).

Fracture domain

$$\theta_f(h) = \vartheta_f(h)[1 - \varphi_f(0)] \quad \varphi_f(0) = \frac{\varphi_b - (1 - \beta_{fk})\varphi_a(0)}{\beta_{fk}} \quad [7b]$$

Bulk soil

$$\theta_b(h) = \beta_{fk}\theta_f(h) + (1 - \beta_{fk})\theta_a(h) \quad [7c]$$

$SHR\beta_k$

Aggregate domain

$$\theta_a(h) = \vartheta_a(h)[1 - \varphi_a(h)] \quad \varphi_a(h) = \frac{e_a(h)}{1 + e_a(h)} \quad [8a]$$

Fracture domain

$$\theta_f(h) = \vartheta_f(h)[1 - \varphi_f(h)] \quad \varphi_f(h) = \frac{\varphi_b - (1 - \beta_{fk})\varphi_a(h)}{\beta_{fk}} \quad [8b]$$

Bulk soil

$$\theta_b(h) = \beta_{fk}\theta_f(h) + (1 - \beta_{fk})\theta_a(h) \quad [8c]$$

$SHR\beta(h)$

Aggregate domain

$$\theta_a(h) = \vartheta_a(h)[1 - \varphi_a(0)] \quad \varphi_a(0) = \frac{e_{a0}}{1 + e_{a0}} \quad [9a]$$

Fracture domain

$$\theta_f(h) = \vartheta_f(h)[1 - \varphi_f(0)] \quad \varphi_f(0) = \frac{\varphi_b - (1 - \beta_{fk})\varphi_a(0)}{\beta_{fk}} \quad [9b]$$

Weight

$$\beta_f(h) = 1 - \frac{\varphi_a(h)}{\varphi_a(0)}(1 - \beta_{fk}) \quad [9c]$$

Bulk soil

$$\theta_b(h) = \beta_f(h)\theta_f(h) + [1 - \beta_f(h)]\theta_a(h) \quad [9d]$$

$SHRcomb$

Aggregate domain

$$\theta_a(h) = \vartheta_a(h)[1 - \varphi_a(h)] \quad \varphi_a(h) = \frac{e_a(h)}{1 + e_a(h)} \quad [10a]$$

Fracture domain

$$\theta_f(h) = \vartheta_f(h)[1 - \varphi_f(h)] \quad \varphi_f(h) = \frac{\varphi_b - [1 - \beta_f(h)]\varphi_a(h)}{\beta_f(h)} \quad [10b]$$

Weight

$$\beta_f(h) = \beta_0 \exp(\kappa h) \quad [10c]$$

Bulk soil

$$\theta_b(h) = \beta_f(h)\theta_f(h) + [1 - \beta_f(h)]\theta_a(h) \quad [10d]$$

In synthesis, opting for the $SHR\beta_k$ approach implies that the hydraulic properties $\theta(h)$ and $K(h)$ of both the domains will change with h , according to the change in the porosity and pore-size distribution of the domains determined by the shrinkage curve of the matrix. By contrast, with the $SHR\beta(h)$ approach the hydraulic properties will remain fixed and the shrinkage curve will be used to change the weight β_f with water content.

In all cases, in this paper the water retention curves $\theta(h)$ for both the domains were described by the equation proposed by van Genuchten (1980):

$$\theta_i(h) = \theta_{r,i} + (\theta_{0,i} - \theta_{r,i}) \left[\frac{1}{1 + (\alpha_{VG,i} |h|)^{n_i}} \right]^{m_i} \quad i = a, f \quad [11]$$

where the subscript i may be for aggregate (a) and fracture (f) domain. The coefficient θ_0 and θ_r are the volumetric water contents at $h = 0$ and $h \rightarrow -\infty$, respectively; α_{VG} (cm^{-1}), n , and m are curve-fitting parameters.

Soil hydraulic conductivity was described by Mualem's model. The model is based on the capillary bundle theory (Mualem, 1976) and relates relative hydraulic conductivity, K_r , to the effective saturation $\text{Se}_i(h) = (\theta_i - \theta_{r,i}) / (\theta_{0,i} - \theta_{r,i})$, by the analytical expression:

$$K_{r,i}(\text{Se}_i) = \frac{K(\text{Se}_i)}{K_{0,i}} = \text{Se}_i^\delta \left[1 - \left(1 - \text{Se}_i^{\frac{1}{m_i}} \right)^{m_i} \right]^2 \quad [12]$$

with the restriction $m = 1 - 1/n$. K_r is the relative hydraulic conductivity, K_0 is the hydraulic conductivity at $h = 0$, and δ is a parameter which accounts for the dependence of the tortuosity and the correlation factors on the water content.

The parameter $K_{0,f}$ may be calculated as (Peters and Klavetter, 1988; Castiglione et al., 2003)

$$K_{0,f} = \frac{K_{0,b} - (1 - \beta_0) K_{0,a}}{\beta_0} \quad [13]$$

$K_{0,b}$ and $K_{0,a}$ may be measured on larger soil blocks (large soil columns or field plots) and small samples, respectively. β_0 represents β_{fR} and β_{fK} under scenarios RGD and SHR β_K and $\beta(0)$ under both the SHR $\beta(h)$ and SHRcomb scenarios, respectively.

Material and Methods

Experimental Dataset

Soil hydraulic property measurements of both the bulk and the aggregate domain of a soil with fractures were performed on soil columns in the laboratory. The soil under study is classified as Fluvent Vertic, with a blocky structure.

Bulk Soil Properties

Experimental data of the hydraulic properties of the bulk soil, $\theta_b(h)$ and $K_b(h)$, were obtained from experiments performed on large blocks of soils. During winter, being sure that the first soil layer was at high water content, six undisturbed soil columns (30-cm diameter and 30-cm length) were sampled in PVC cylinders from the soil surface in the field. The columns were analyzed for soil

bulk density, saturated water content, and saturated hydraulic conductivity of the bulk soil at the swelling state. Saturated hydraulic conductivity was determined by constant head method (Klute and Dirksen, 1986).

Starting from complete saturation, a drying process (by evaporation) of the soil profile was monitored for each column by two TDR probes and two tensiometers installed horizontally at depths of 10 and 20 cm, as well as by measuring column weights. The TDR transmission line consisted of an antenna cable (RG58, 50 Ω characteristic impedance, 210 cm long, and with 0.2 Ω connector impedance) and of three-wire probes, 15 cm long, 3-cm internal distance, 0.3 cm in diameter. Tensiometers consisted of ceramic cups, 25 mm in diameter and 25 cm long, connected to a mercury manometer.

The water retention curve for the bulk soil was obtained from the experimental $\theta(h)$ values by plotting pairs of water contents and pressure heads at the two depths, measured during the drying process. At the end of the drying process, which lasted about 3 wk, shrinkage macrofractures could be observed at the soil surface.

Aggregate Domain Soil Properties

After the winter, when macrofractures became visible by the naked eye at the soil surface in the field, 18 smaller undisturbed soil samples (15-cm length and 10-cm diameter) were carved by stainless-steel cylinders at the surface of the matrix polygons bordered by cracks. In the laboratory, steel samplers were removed, and the soil cores were wrapped with flexible rubber except at the top and bottom. The soil cores were then slowly saturated with a conditioning solution (CaSO_4 0.025M) by wetting from the bottom. Saturated hydraulic conductivity was determined by using a constant head permeameter (Klute and Dirksen, 1986).

A state of hydrostatic equilibrium was then induced ($h = 0$ cm at the surface and $h = +15$ cm at the bottom) setting a zero flux at the bottom surface. An evaporation experiment (Wind, 1968), with the modifications suggested by Garnier et al. (1997), was performed during 3 to 4 d by drying the soil (i.e., evaporation was supported with a small fan positioned near the top) with the lower end of the soil core completely sealed. Column weight and pressure heads were continuously monitored with a strain-gauge load cell (range from 0 to 3 kg and a precision of ± 1 g) and tensiometers (length = 3 cm, diameter = 0.5 cm, bubbling pressure head = -800 cm), respectively, installed horizontally at 5 and 10 cm from the bottom. Column diameter and height were measured three times each day by measuring three marked surfaces and three vertical positions with an electronic caliper (precision of 0.05 mm). The experimental procedure performed for another site is described in detail in Coppola et al. (2012). The procedure allowed experimental points of the three soil functions, $\vartheta_a(h)$, $K_a(\vartheta_a)$, and $e_a(h)$, to be simultaneously determined.

Data Handling

Under conditions RGD, $\text{SHR}\beta_k$, $\text{SHR}\beta(h)$, and SHRcomb , the $\vartheta_a(h)$, $K_a(\vartheta_a)$, and $e_a(h)$ experimental data points measured on the soil cores (the average of the 18 cores), as well as $\theta_b(h)$ measured on the large columns (the average of the six columns) were converted to as many $\theta_a(h)$, $K_a(\theta_a)$ points for the aggregate domain and to as many $\theta_f(h)$ and $K_a(\theta_f)$ for the fracture domain as follows:

RGD

1. Since it is assumed that the aggregate domain is not shrinking and thus its porosity is constant, soil moisture ratios, $\vartheta_a(h)$, values, measured on the aggregate domain, were converted to volumetric water retention, $\theta_a(h)$ values, by fixing $e_a(h)$ at the value measured at saturation, $e_a(0)$ (Eq. [7a]). Equation [11] was fitted to the $\theta_a(h)$ values to estimate the water retention parameters for the aggregate domain.

2. Weight β_f was set at a constant value ($\beta_f = \beta_{fR}$).

3. The corresponding $\theta_f(h)$ values (at the same h) were calculated by Eq. [7b].

4. The parameters of the water retention curve for the fracture pore domain, $\theta_f(h)$, and parameter β_{fR} were estimated by fitting Eq. [7c] (with $\theta_a(h)$ and $\theta_f(h)$ given by Eq. [7a] and [7b], respectively) to the measured bulk volumetric water retention data, $\theta_b(h)$, coming from the large columns. The number of fitting parameters was reduced by fixing the parameters for $\theta_a(h)$ in Eq. [7c] at those estimated on the soil cores in Step 1 above. This way, the parameters of the hydraulic properties for the fracture may be estimated more robustly.

5. Finally, $K_{0,fR}$ and $K_{fR}(\text{Se})$ were estimated by applying Eq. [13] and [12], respectively, by fixing $K_{0,a}$ and $K_{0,b}$ at the measured values and setting $\beta_0 = \beta_{fR}$.

$\text{SHR}\beta_k$

1. Now soil moisture ratios, $\vartheta_a(h)$ values, measured on the aggregate domain, were converted to volumetric water retention, $\theta_a(h)$ values, by using the $e_a(h)$ value actually measured at each h (Eq. [8a]). Again, Eq. [11] was fitted to the $\theta_a(h)$ values to estimate the water retention parameters for the aggregate domain.

2. Weight β_f was set at a constant value ($\beta_f = \beta_{fk}$).

3. The corresponding $\theta_f(h)$ values (at the same h) were calculated by Eq. [8b].

4. The parameters of the water retention curve for the fracture pore domain, $\theta_f(h)$, and the parameter β_{fk} , were estimated by fitting Eq. [8c], with $\theta_a(h)$ and $\theta_f(h)$ given by Eq. [8a] and [8b], respectively, to the measured bulk volumetric water retention data, $\theta_b(h)$, coming from the large columns. The parameters for

$\theta_a(h)$ in Eq. [8c] were fixed to those estimated on the soil cores in Step 1 of this $\text{SHR}\beta_k$ case.

5. Finally, $K_{0,fk}$ and $K_{fk}(\text{Se})$ were estimated by applying Eq. [13] and [12], respectively, by fixing $K_{0,a}$ and $K_{0,b}$ at the measured values and setting $\beta_0 = \beta_{fk}$.

$\text{SHR}\beta(h)$

1. Something in between cases RGD and $\text{SHR}\beta_k$. Indeed, soil moisture ratios, $\vartheta_a(h)$, were converted to volumetric water retention, $\theta_a(h)$ values, by fixing $e_a(h)$ at the value measured at saturation, $e_a(0)$ (Eq. [9a]). Again, as in the RGD case, Eq. [11] was fitted to the $\theta_a(h)$ values to estimate the water retention parameters for the aggregate domain.

2. The corresponding $\theta_f(h)$ values (at the same h) were calculated by Eq. [9b].

3. The information on changing pore distribution during aggregate deformation, $e_a(h)$, was now used to calculate points of the $\beta(h)$ curve (Eq. [9c]).

4. The parameters of the water retention curve for the fracture pore domain, $\theta_f(h)$, and parameter β_{fk} , were estimated by fitting Eq. [9d], with $\theta_a(h)$, $\theta_f(h)$, and $\beta(h)$ given by Eq. [9a], [9b], and [9c], respectively, to the measured bulk volumetric water retention data, $\theta_b(h)$, coming from the large columns. The parameters for $\theta_a(h)$ in Eq. [9d] were fixed to those estimated on the soil cores in Step 1 of this $\text{SHR}\beta(h)$ case.

5. Finally, $K_{0,f\beta(h)}$ and $K_{f\beta(h)}(\text{Se})$ were estimated by applying Eq. [13] and [12], respectively, by fixing $K_{0,a}$ and $K_{0,b}$ at the measured values and setting $\beta_0 = \beta_f(0) = \beta_{fk}$.

SHRcomb

1. Something in between cases $\text{SHR}\beta_k$ and $\text{SHR}\beta(h)$. Soil moisture ratios, $\vartheta_a(h)$, measured on the aggregate domain, were converted to volumetric water retention, $\theta_a(h)$ values, by using the $e_a(h)$ value measured at each h (Eq. [10a]). Equation [11] was fitted to the $\theta_a(h)$ values to estimate the water retention parameters for the aggregate domain.

2. The corresponding $\theta_f(h)$ values (at the same h) were calculated by Eq. [10b].

3. The parameters of the water retention curve for the fracture pore domain, $\theta_f(h)$, and the parameter of the $\beta(h)$ curve (Eq. [10c]), were estimated by fitting Eq. [10d], with $\theta_a(h)$, $\theta_f(h)$, and $\beta(h)$ given by Eq. [10a], [10b], and [10c], respectively, to the measured bulk volumetric water retention data, $\theta_b(h)$, coming from the large columns. The parameters for $\theta_a(h)$ in Eq. [10d] were fixed to those estimated on the soil cores in step 1 of this SHRcomb scenario.

4. Finally, $K_{0,f\beta}(b)$ and $K_{f\beta}(b)(Se)$ were estimated by applying Eq. [13] and [12], respectively, by fixing $K_{0,a}$ and $K_{0,b}$ at the measured values and setting $\beta_0 = \beta_f(0) = \beta_{fk}$.

Numerical Simulations

The purpose of simulations was mainly to compare the water flow and solute transport behavior in a wide range of water contents, from saturation to drier conditions, under the RGD and the SHR dual-permeability hydraulic parameterizations. The specific objective was to show the impact of matrix volume changes on water storage, water fluxes, and solute concentrations during an infiltration process bringing an initially dry soil to saturation and a drainage process starting from an initially saturated soil.

Numerical simulations were performed by considering a single-layer, 150 cm-deep soil profile and a time interval of 2 and 5 h for the infiltration and drainage processes, respectively. As for the infiltration, we assumed a potential-type top boundary condition ($b = 0$ cm). For the drainage process, we assumed a zero-flux flow top boundary condition. A unit hydraulic gradient (free drainage) was assumed as the bottom boundary condition at the 150-cm depth for both the pore domains. The profile was assumed to be initially at a constant pressure head of $b = -400$ cm and $b = 0$ cm for the infiltration and the drainage processes, respectively, in both domains.

As for solute transport, a finite pulse of solute of 0.5 g cm^{-3} , lasting 0.01 h, was applied at the top boundary at the beginning of the simulation period for the infiltration process. The initial condition was assumed to be a zero concentration. For the drainage process, no solute was applied at the surface. The initial condition was assumed to be a constant concentration $C = 0.001 \text{ g cm}^{-3}$ in both the domains. In both the infiltration and the drainage processes simulation, a zero concentration gradient was imposed at the bottom boundary, thus allowing solute to leave the profile with draining water.

Water and solute transfer coefficient, α_w and α_s were assumed to be $1\text{E-}04 \text{ cm}^{-1} \text{ h}^{-1}$ and $1\text{E-}04 \text{ h}^{-1}$, respectively. The dispersivity was assumed to be $\lambda = 5$ cm and $\lambda = 1$ cm for the fracture and aggregate domains, respectively.

The water flow processes simulated in this study were simulated by a MathLab numerical code based on a standard finite difference scheme (Coppola and Randazzo, 2006; Coppola et al., 2012). In the model, vertical transient flow is simulated by numerically solving the one-dimensional form of the Richards equation (in a dual-permeability configuration) using an implicit, backward, finite differences scheme with explicit linearization (see Appendix A in Coppola et al., 2012). An explicit, central finite difference scheme is used to solve advection–dispersion equations (Coppola et al., 2014).

The simulations were performed by assuming either hydraulic properties accounting for soil shrinking, both $\text{SHR}\beta_k$ and $\text{SHR}\beta(h)$, or a rigid soil (RGD) with a constant β_{FR} .

By considering the SHR cases, the code works as for the case of a rigid dual-permeability model except that the hydraulic function parameters now account for the swell–shrink dynamics. Additionally, under the $\text{SHR}\beta(h)$ and the SHRcomb assumptions, $\beta_f(h)$ has to be evaluated at each numerical node according to the bulk pressure head values.

Results

Porosities, Fracture Domain Weight and Hydraulic Properties under the Rigid (RGD) and Shrinking (SHR) Hypotheses

The graph in Fig. 2a shows the $e_a(h)$ curve as the average (CV: $e_{a0} = 4.5\%$, $e_{ar} = 6.0\%$, $\alpha_e = 6.0\%$, $n_e = 5\%$) of the experimental shrinkage characteristics measured on the soil cores. The aggregate porosity, calculated on the soil cores curve (Fig. 2b, solid line), changes from $\varphi_a = 0.365$ to $\varphi_a = 0.294$ ($\sim 19\%$) in the pressure head range $b = 0$ to -400 cm.

Figure 3a,b,c,d shows the water retention and the hydraulic conductivity curves obtained for the aggregate and the fracture domains under scenarios RGD and SHR. In Fig. 3a,b the cross symbols represent the experimental water retention points obtained on the bulk soil from the large column tests, averaged from the six columns. Bulk porosity was assumed to be equivalent to the water content measured at $b = 0$ in the large column tests. An average

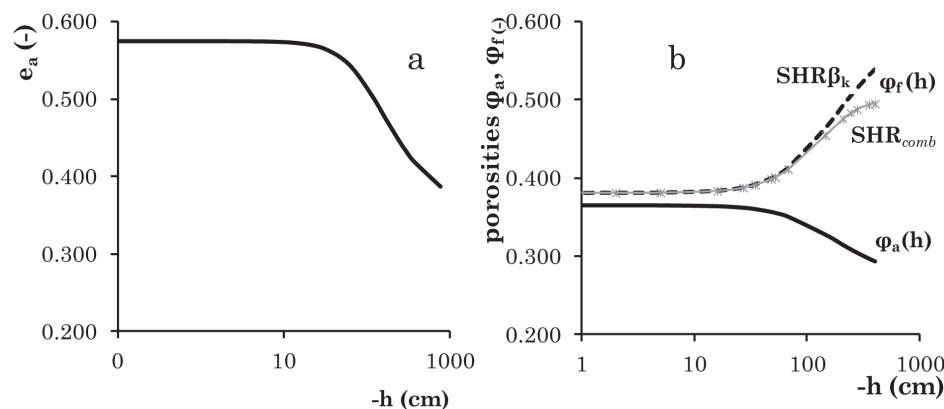


Fig. 2. (a) Void ratio, e_a , versus pressure head, b , measured on the small undisturbed soil samples. (b) Corresponding dynamic of porosity with the pressure head for the aggregate and fracture domains. The curves represent averages of the measurement (aggregate domain) and estimates (fracture domain) coming from the 18 soil samples investigated.

bulk porosity $\varphi_b = 0.370$ was found, hence very close to the average aggregate porosity, φ_a , measured on the soil cores. The average bulk water retention curve was described by alternatively assuming either a RGD or a SHR aggregate domain porous medium.

Table 1 reports the parameters for both the fracture and aggregate domains under the different scenarios. The parameters for the fractures were obtained by fitting Eq. [7c], [8c], and [9d] to the bulk water retention experimental points measured on the large columns, while fixing the parameters for the aggregate domain to those estimated on the soil cores. Optimization was conducted by using different combinations of starting values. The “global” minimum was detected in correspondence with the parameter vector on which the majority of runs converged. R^2 for the fitting was 0.99 for the two SHR and the RGD cases.

Looking at the graphs in Fig. 3, we first compare the water retention curves for the RGD (solid black lines) and the $\text{SHR}\beta_k$ scenarios (dashed lines plus circles). First, it may be seen that assuming the rigidity of the two domains leads to a physically implausible water retention functions for the two domains, with the n_{VG} parameter higher for the aggregate domain and more similar to that of a clay soil for the fracture domain. Accounting for aggregate domain deformation in the $\text{SHR}\beta_k$ scenario has the effect of lowering both the air entry pressure head (higher α_{VG}) and the n_{VG} parameters in the aggregate domain. This change in the aggregate domain is counterbalanced by the opposite change in the water retention

parameters of the fracture domain and by a change in the weight of the fracture domain ($\beta_{fR} = 0.350$ and $\beta_{fk} = 0.311$). Now the α_{VG} and the n_{VG} parameters are very similar for both domains, a fact that appears to be still somehow questionable.

These changes have obvious consequences on the hydraulic conductivity curves. The slope of the $\text{SHR}\beta_k$ curve suggests more gradual emptying of the aggregate porous medium and more rapid emptying of the fracture domain. This has effects throughout the hydraulic conductivity curves, which become significantly lower for the aggregate domain and higher for the fracture domain. As for hydraulic conductivity at saturation, the different weight changes $K_{0fR} = 46 \text{ cm h}^{-1}$ to $K_{0fk} = 51 \text{ cm h}^{-1}$.

Looking at the $\text{SHR}\beta(h)$ curves (dashed lines plus triangles), the water retention and hydraulic conductivity behavior combines those of the two RGD and $\text{SHR}\beta_k$ extremes. Obviously, the water retention and the hydraulic conductivity curves coincide with the curves of the RGD case. By contrast, those for the fracture domains mostly overlap the curves obtained under the $\text{SHR}\beta_k$ condition. This behavior immediately comes from the assumptions we made to deduce the $\beta(h)$ curve (Eq. [4a–4d] and [9a–9c]).

For the same assumptions, the β_{fk} value obtained for the $\text{SHR}\beta_k$ case represents the lower limit for the $\beta(h)$ curve under the $\text{SHR}\beta(h)$ scenario, $\beta(0) = \beta_{fk}$. Thus, $K_{0f\beta(h)} = K_{0fk}$. The average $\beta(h)$ curve obtained under this scenario is depicted in Fig. 4

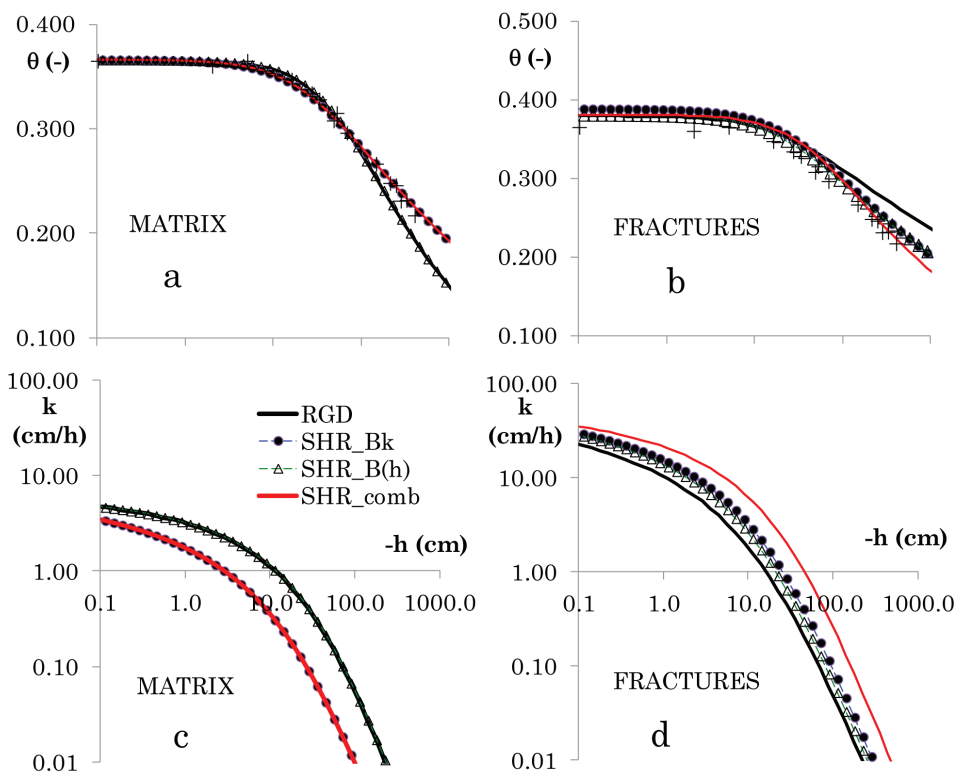


Fig. 3. Water retention and hydraulic conductivity curves obtained for the aggregate and the fracture domains under the RGD and the SHR scenarios. In Fig. 3a,b the cross symbols represents the experimental water retention points obtained on the bulk soil from the large column tests, as average of values from the six columns.

Table 1. Parameters for both the fracture and the aggregate domains under the four scenarios. The parameters for the fractures were obtained by fitting Eq. [7c], [8c], [9d], and [10d] to the bulk water retention experimental points measured on the large columns, while fixing the parameters for the aggregate domain to those estimated on the soil cores. β_{f0} represents, respectively, the β_{fR} , the β_{fk} and the $\beta_f(h)$ values under the four scenarios.

		θ_0	θ_r	α_{VG}	n_{VG}	K_0	τ	β_{f0}
RGD	fractures	0.379	0.000	0.045	1.129	45.976	-1.000	0.350
	aggregates	0.366	0.000	0.022	1.304	6.013	-1.000	
SHR β_k	fractures	0.388	0.000	0.039	1.185	50.987	-1.000	0.311
	aggregates	0.366	0.000	0.041	1.179	6.013	-1.000	
SHR $\beta(h)$	fractures	0.381	0.000	0.045	1.170	50.987	-1.000	0.311
	aggregates	0.366	0.000	0.022	1.304	6.013	-1.000	
SHRcomb	fractures	0.381	0.000	0.025	1.236	50.987	-1.000	0.311
	aggregates	0.366	0.000	0.041	1.179	6.013	-1.000	

(dashed line). It suggests an exponential evolution of the weight with the log-pressure head. The parameters for the fracture and the aggregate domains follow a behavior similar to that observed in the RGD scenario, with a reversed behavior of the n_{VG} parameter, higher for the aggregate domain.

Under the SHRcomb scenario, the curves (solid red lines) and the corresponding parameters move to a more physically plausible region. The n_{VG} parameter is now higher for the fracture domain, which is what one expects for a faster flow domain. This shifts the hydraulic conductivity curve for the fracture domain significantly upward. Obviously, the water retention and the hydraulic conductivity curves (and the corresponding parameters) overlap the curves obtained under the SHR β_k scenario. The $\beta(h)$ curve obtained under this scenario (solid line in Fig. 4) still follows an exponential evolution of the weight with the log-pressure head, but with different parameters compared to the SHR $\beta(h)$ scenario.

Numerical Simulations

For the sake of clarity, we will separately consider the simulation results on water content, solute concentrations, and water fluxes obtained under the different RGD and SHR scenarios. We recall that simulations refer to an infiltration process bringing an initially

dry soil to saturation and a drainage process starting from an initially saturated soil. In all cases we will first show the simulations of the infiltration process and then the simulations of the drainage process.

Let it be understood that water contents, concentrations, and fluxes of the bulk soil were obtained after multiplication of the fracture and matrix contributions by their relative volumes, i.e., β_f and $(1 - \beta_f)$.

Water Contents, Water Exchange Term, and Weight

Infiltration. The water content profiles obtained under the different conditions are depicted separately in Fig. 5 for the aggregate and fracture domains. The graphs in the right column of the figure summarize the results of the bulk soil for all four simulation scenarios.

With regard to the RGD scenario, the graphs for the infiltration process show a fairly classical propagation of the wetting fronts, resembling behavior that is typical of a uniform soil in both domains. The fronts move more or less with the same shape in both the matrix and the fracture domains, with the fracture wetting front only a little faster due mostly to the significantly higher α_{VG} and K_0 parameters. As stated above, this makes the RGD scenario physically implausible, as in a dual-permeability context one logically expects the coexistence of significantly slower and faster flow domains. The RGD exchange term, Γ/β_f of water between domains (lines in Fig. 6) propagates with depth as a sort of pulse, starting and ending in a depth range of about 30 cm and with a peak value increasing with depth due to the increasing distance with time between the wetting fronts in the matrix and the fracture domains. In the graph, positive values indicate water transfer from fractures to the aggregate domain.

Under the SHR β_k scenario, the relative velocity of wetting front propagation changes significantly. The front now moves much more rapidly in the fractures. The water content in the matrix increases only relatively slowly, and mostly through the exchange

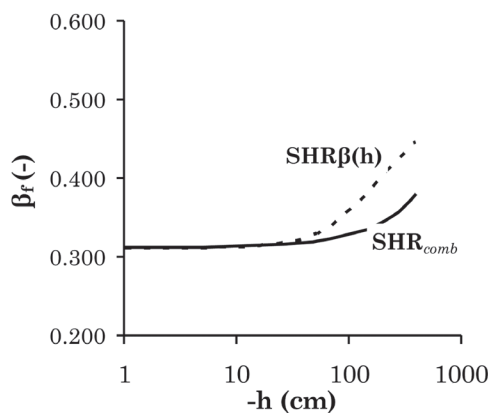


Fig. 4. $\beta(h)$ curve under the SHR $\beta(h)$ and the SHRcomb scenarios.

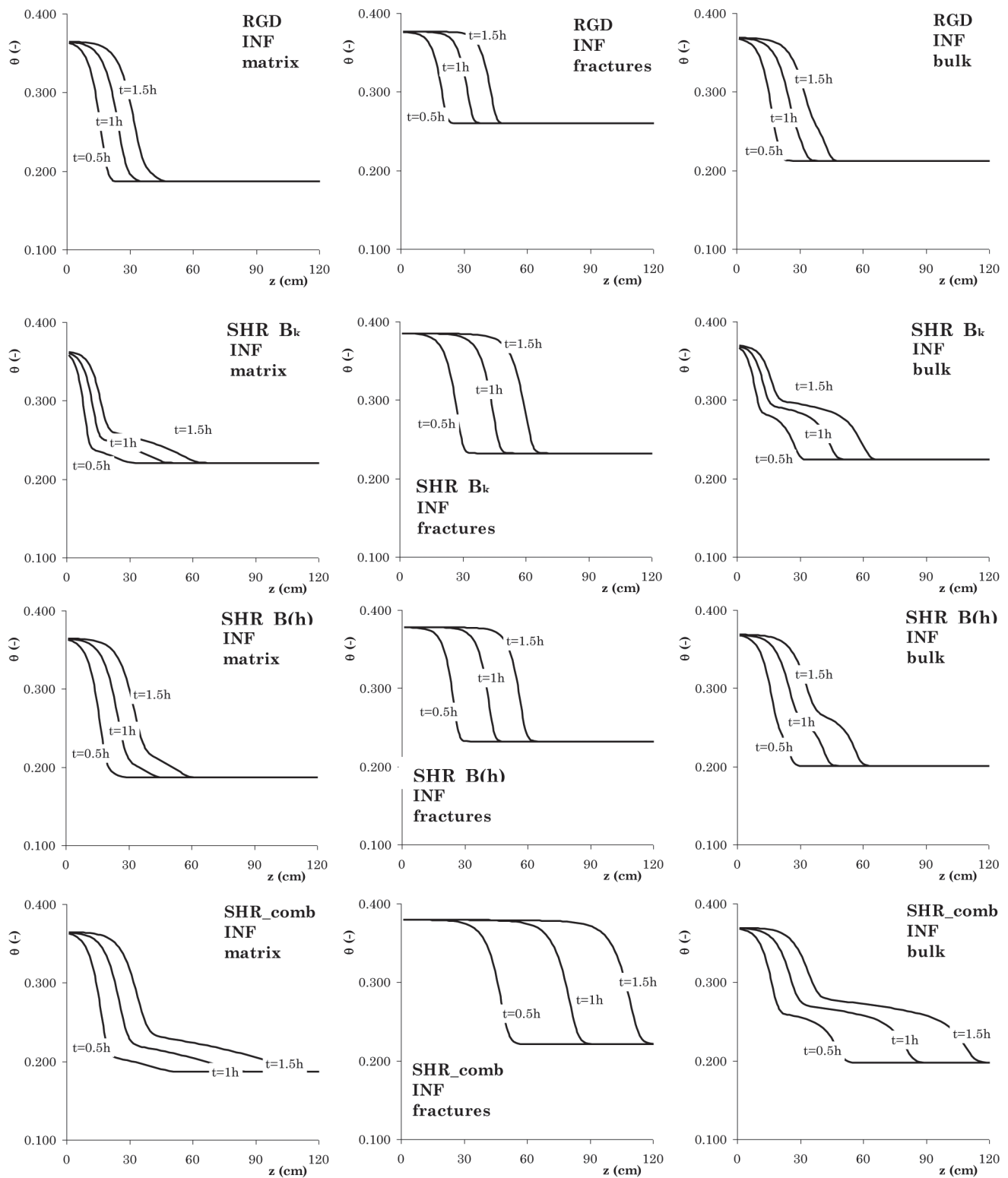
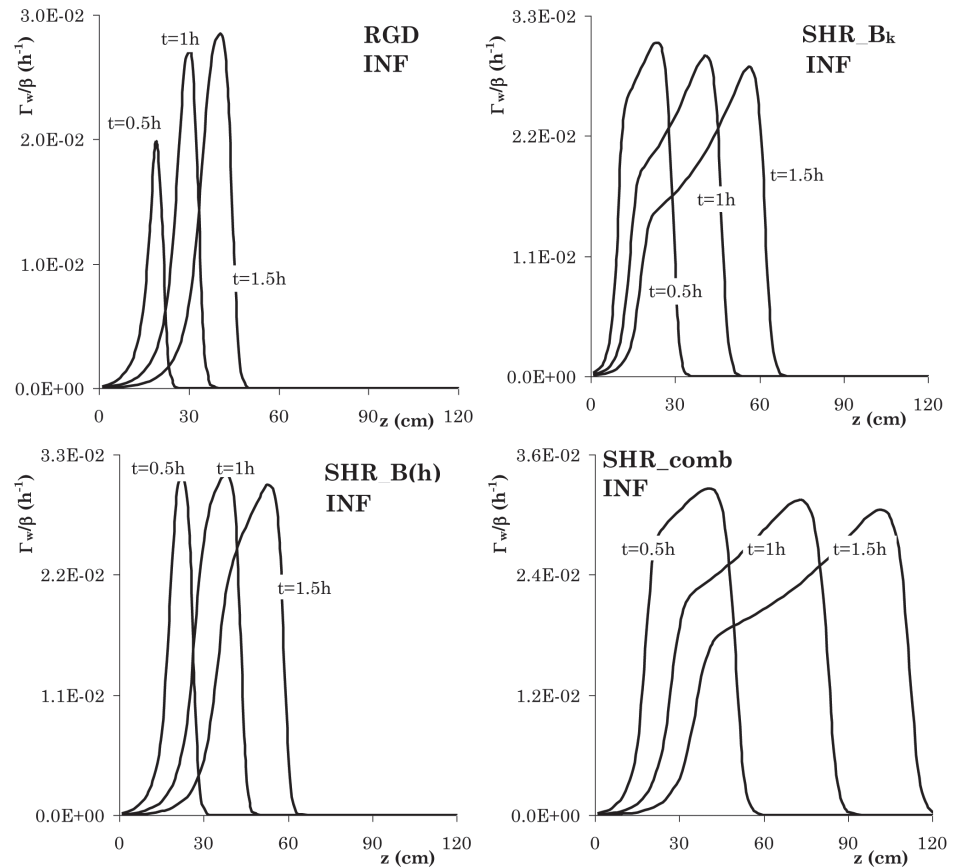


Fig. 5. Water content profiles obtained under the different conditions, separately for the matrix and the fracture domains, for the infiltration process. The graphs in the last column in the figure summarize the results of the bulk soil for all the simulation scenarios.

of water from the fractures. Indeed, for this scenario, the exchange term (Fig. 6) increases dramatically at the passage of the fast fracture front. The exchange propagates downward faster than in the

RGD scenario and gradually expands, involving increasing depth intervals over time, which explains the increase in water content observed in the matrix domain far beneath the wetting front.

Fig. 6. Depth–time evolution of water transfer from the fracture to the matrix domain simulated under the different scenarios for the infiltration process



As for the $\text{SHR}\beta(h)$ scenario, the wetting front propagation in the matrix resembles that observed in the RGD case, whereas the front in the fractures is much more similar to that observed in the $\text{SHR}\beta_k$ scenario. This was largely expected, given that under the $\text{SHR}\beta(h)$ scenario the aggregate domain hydraulic properties coincide with the RGD aggregate properties and the fracture hydraulic properties practically overlap those of $\text{SHR}\beta_k$.

As a consequence, the exchange term (Fig. 6) takes on a behavior in between RGD and $\text{SHR}\beta_k$, as it propagates downward a little faster than in the RGD case, but the shape beneath the front is more similar to that of $\text{SHR}\beta_k$.

Under the SHR_{comb} scenario, the propagation velocity of the wetting front in the fracture domain is at least twice that observed in all the other scenarios and significantly higher than in the aggregate domain. This behavior comes from the more plausible hydraulic parameters obtained in this case (see Table 1) and makes this scenario much more realistic from a physical point of view. Overall, it is the behavior expected for a fractured porous medium, typically characterized by a faster fracture domain and a slower matrix domain. The shape of the exchange term with depth resembles that observed under the $\text{SHR}\beta_k$ scenario but is now much faster and involves much larger depth intervals.

The shape of the water content profiles in the bulk soil (Fig. 5, right column) results from the combination of the aggregate and fracture domain water contents.

In general, under the RGD scenario, the bulk soil wetting front appears quite uniform, due to the similar propagation velocity of the front in the two domains. By contrast, under the SHR scenarios, the wetting front takes a bimodal shape, as the front in the matrix follows far behind that in the fracture domain, and hence the two fronts cross a given depth plane at a relatively distant time. In general, the shallower and deeper parts of the bimodal front come from the aggregate and fracture contributions, respectively.

Drainage. During drainage, the water content evolution is practically overlapping under scenarios RGD, $\text{SHR}\beta_k$, and $\text{SHR}\beta(h)$ (see Fig. 7). Under the SHR_{comb} scenario, the shape remains similar to that observed in the other cases, but the drainage appears to be more accelerated, as both domains lose water more rapidly.

In all cases, drainage in practice occurs under steady-state conditions, and the soil profile loses water quite uniformly, as confirmed by the shape of the water content profiles, which are almost parallel over time. Probably no nonequilibrium conditions developed because of the sufficiently large mass exchange as compared to the flow rates.

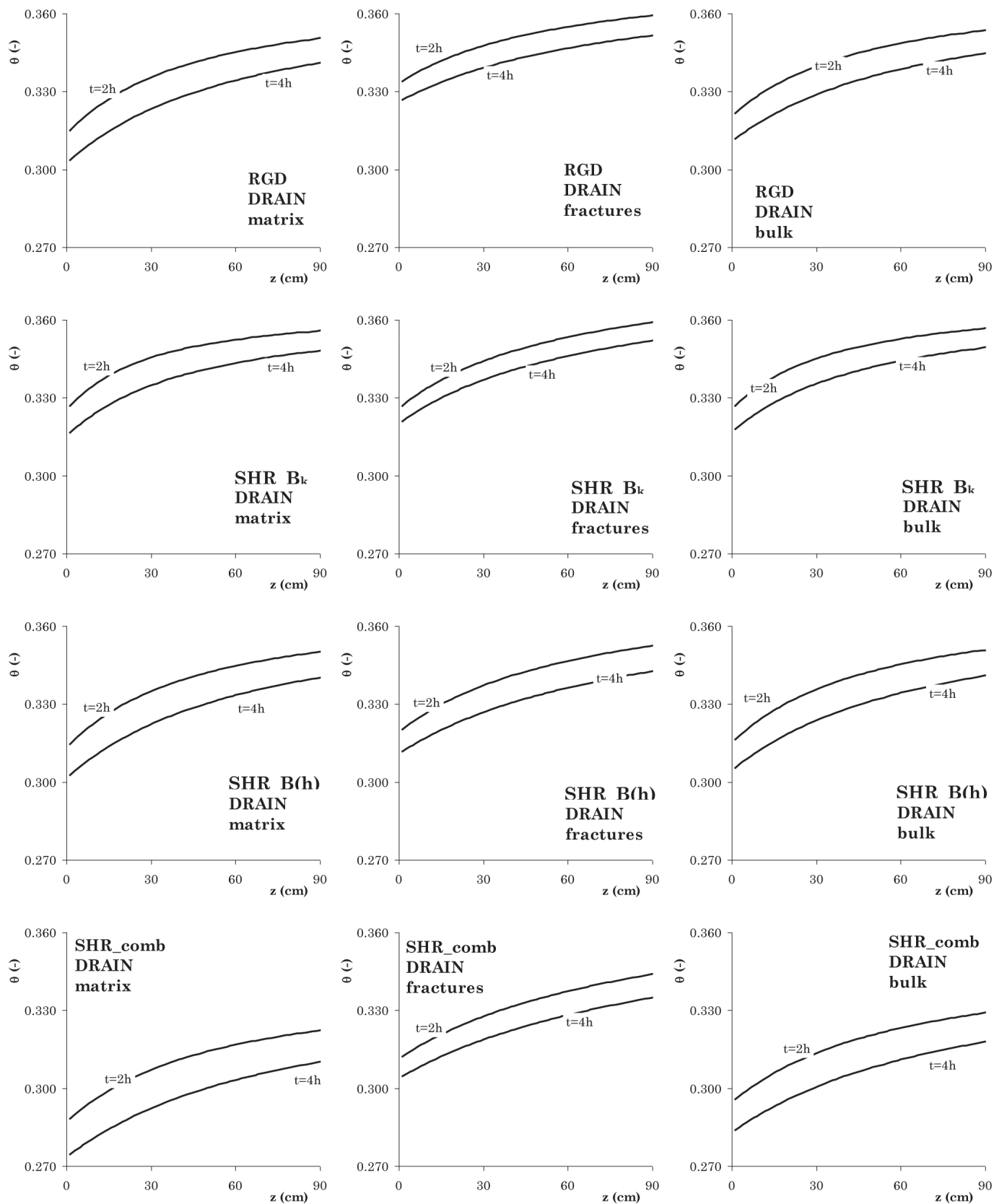


Fig. 7. Water content profiles obtained under the different conditions, separately for the matrix and the fracture domains, for the drainage process. The graphs in the last column in the figure summarize the results of the bulk soil for all the simulation scenarios.

The similar shape of the drainage water content profiles hides a significantly different exchange term under the four scenarios (see Fig. 8). In the RGD scenario, the exchange term assumes positive values in the shallower part of the soil profile (water moves from the fracture to the aggregate domain), while in the deeper part the fractures receive water from the matrix (negative values of the exchange term). In the SHR scenarios, water moves everywhere from the aggregate to the fracture domain but still with a different shape. In $\text{SHR}\beta_k$ and SHRcomb , the exchange is higher (more negative values) at the surface and decreases with depth. The exchange magnitude is also similar. In the $\text{SHR}\beta(h)$ scenario the exchange term oscillates with depth and is one order of magnitude lower than in the $\text{SHR}\beta_k$ and the SHRcomb scenarios.

To be exhaustive, the graphs in Fig. 9 depict the behavior of the weight β under scenarios $\text{SHR}\beta(h)$ and SHRcomb , which are the only cases where β changes with the pressure head, h , for both the infiltration and drainage processes. Interestingly, at least in the range of pressure heads investigated, the depth-profile of the weight assumes a bimodal shape during the infiltration process (more accentuated in the SHRcomb scenario), due to the different depth location of the aggregate and fracture wetting front along the soil profile. This bimodal profile propagates gradually downward during the infiltration process, bringing the weight to the β_0 value with the progressive saturation of the soil profile.

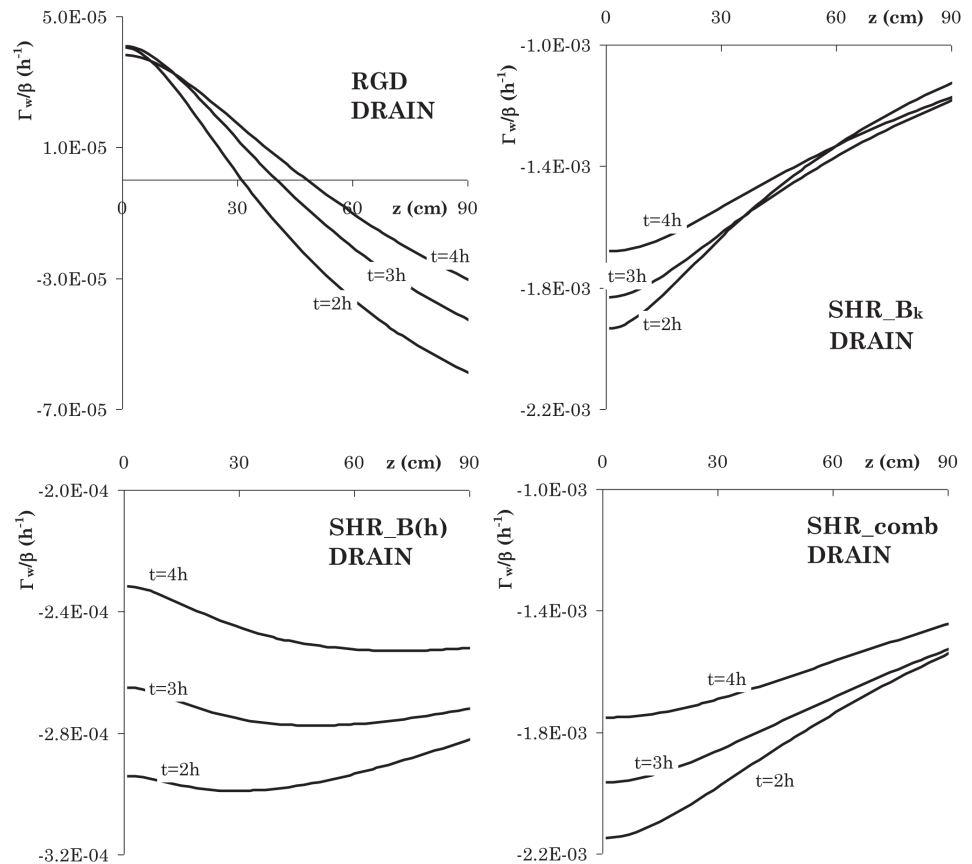
By contrast, during the drainage process the weight assumes a unimodal shape. The weight dynamics with depth is apparent in the $\text{SHR}\beta(h)$ scenario, whereas it is only faint in SHRcomb , the latter behavior suggesting a relatively more uniform drainage of the soil profile.

Solute Concentrations and Solute Exchange Term

Infiltration. Similar to the water contents, Fig. 10 depicts the concentration profiles obtained under the different scenarios, separately for the aggregate and fracture domains. Again, the graph in the right-hand column summarizes the results of the bulk soil for all three simulation scenarios. In general, concentrations in the aggregate and fracture domains tend to differ because of the different propagation velocities of the wetting front, the different dispersivities used for the two domains ($\lambda = 1$ cm for the matrix and $\lambda = 5$ cm for the fracture domain) and the different mass entering each domain, which is related to the flux of water at the soil surface. This, in turn, depends on the different hydraulic properties of the two domains. We recall that a pulse of solute of 0.5 g cm^{-3} , lasting 0.01 h, was applied at the beginning of the simulation period.

Under scenarios RGD, $\text{SHR}\beta_k$, and $\text{SHR}\beta(h)$, the concentration distribution propagates downward with a similar shape and a similar concentration peaks in the fracture domain. The propagation velocity is a little lower in the RGD scenario. By contrast,

Fig. 8. Depth-time evolution of water transfer from (positive values) and to (negative values the fracture domain simulated under the different scenarios for the drainage process.



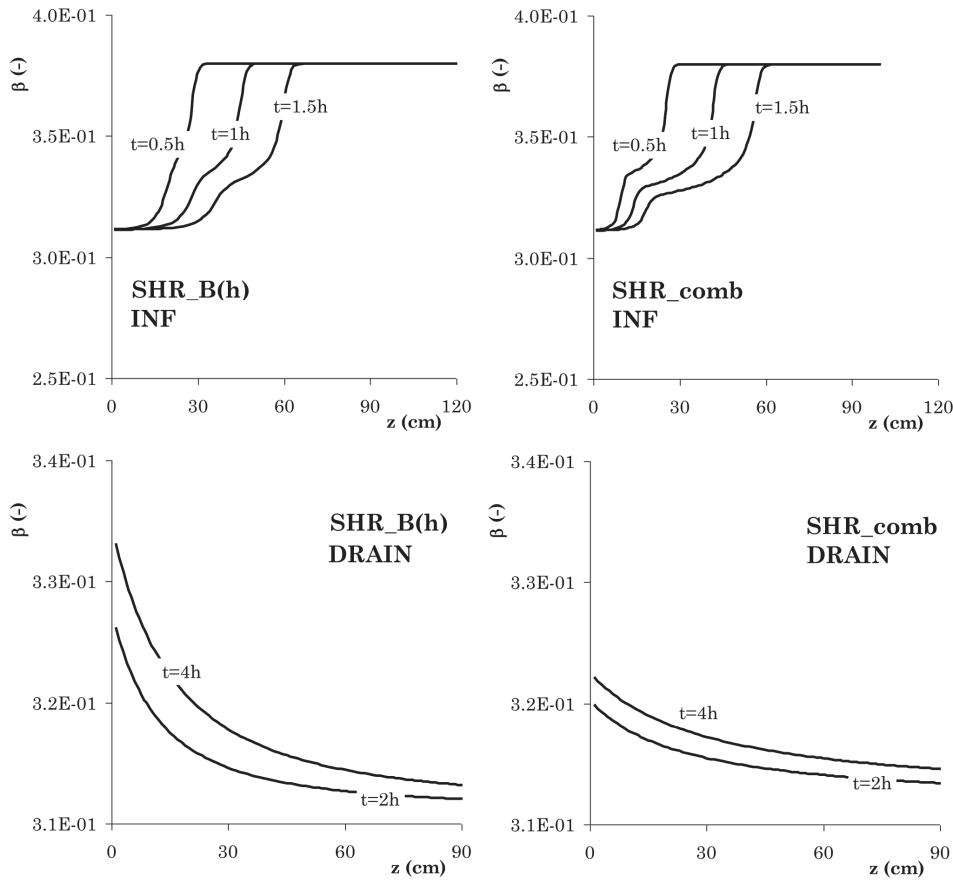


Fig. 9. Evolution of weight β under the $\text{SHR}\beta(h)$ and the SHRcomb scenarios, for both the infiltration (top panel) and the drainage (bottom panel) processes.

the concentration evolution is significantly different in the aggregate domain. The low peak concentrations observed in RGD and $\text{SHR}\beta(h)$ at the larger times, compared to the higher peaks observed in scenario $\text{SHR}\beta_k$ at the same times, has to be related to the higher water contents induced by the faster propagation velocity of the RGD and the $\text{SHR}\beta(h)$ wetting fronts in the aggregate domains (Fig. 5).

The similar evolution of RGD, $\text{SHR}\beta_k$, and $\text{SHR}\beta(h)$ concentrations is reflected in the similar shape of the solute exchange term in the three scenarios (Fig. 11). The solute exchange profile propagates downward as a sort of pulse with a peak magnitude gradually decreasing but widening on larger depth intervals over time.

As for the SHRcomb scenario, despite the different concentration magnitude, the concentration profiles in the aggregated and fracture domains propagate at the same velocity with depth. As the wetting fronts are characterized by very different velocities (Fig. 5), the concentration magnitude, the depth extent of the concentration profile, as well as its dynamics, in the aggregate domain may only be explained by the magnitude, depth extent, and dynamics of the solute exchange from the fracture to the aggregate domain. The SHRcomb solute exchange profile propagates with depth with a trend similar to those observed in the other scenarios, but now with a significantly larger magnitude of the solute exchange values and with depth intervals involved that are more or less twice those

observed in the other three scenarios, a behavior already observed for the water exchange.

As for the bulk concentrations, the SHRcomb scenario deviated the most from the RGD case, showing the earliest solute propagation, with the largest concentrations. By contrast, due to the similarity of both the concentration profiles in the fracture domain and the solute exchange term, the bulk concentration magnitude and propagation in the $\text{SHR}\beta_k$ and the $\text{SHR}\beta(h)$ scenarios were mostly similar (only a little faster) to the RGD concentrations.

Drainage. As for the drainage process (Fig. 12), in general the concentration in the aggregate domain increases with time because of the solute exchange from the fractures. In both domains, the concentration changes steadily over time, as indicated by the practically parallel depth concentration profiles. However, the depth evolution of concentrations changes with the scenario considered. The solute concentrations appear to be quite uniform along the soil profile under the $\text{SHR}\beta_k$ and the SHRcomb scenarios. A more varied profile may be observed in the RGD and the $\text{SHR}\beta(h)$ scenarios, characterized by a shallow depth interval where concentrations change rapidly with depth, followed by a fairly uniform concentration deeper in the soil profile. The particular concentration profile observed in the aggregate domain under the RGD scenario may be explained through the causal relationship between the concentrations and the solute exchange term. While the solute

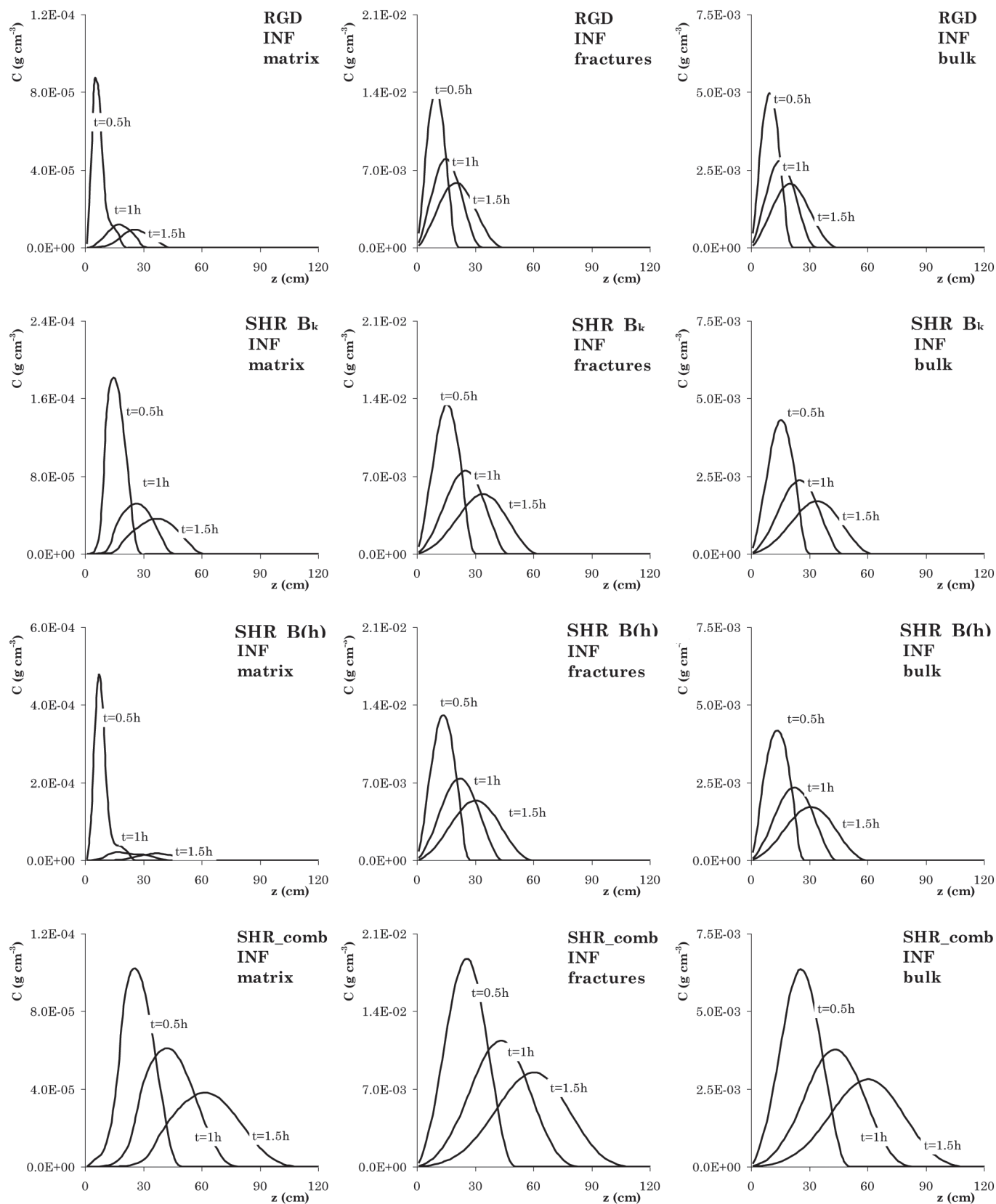


Fig. 10. Concentration profiles obtained under the different conditions, separately for the matrix and the fracture domains, for the infiltration process. The graphs in the last column in the figure summarize the results of the bulk soil for all the simulation scenarios.

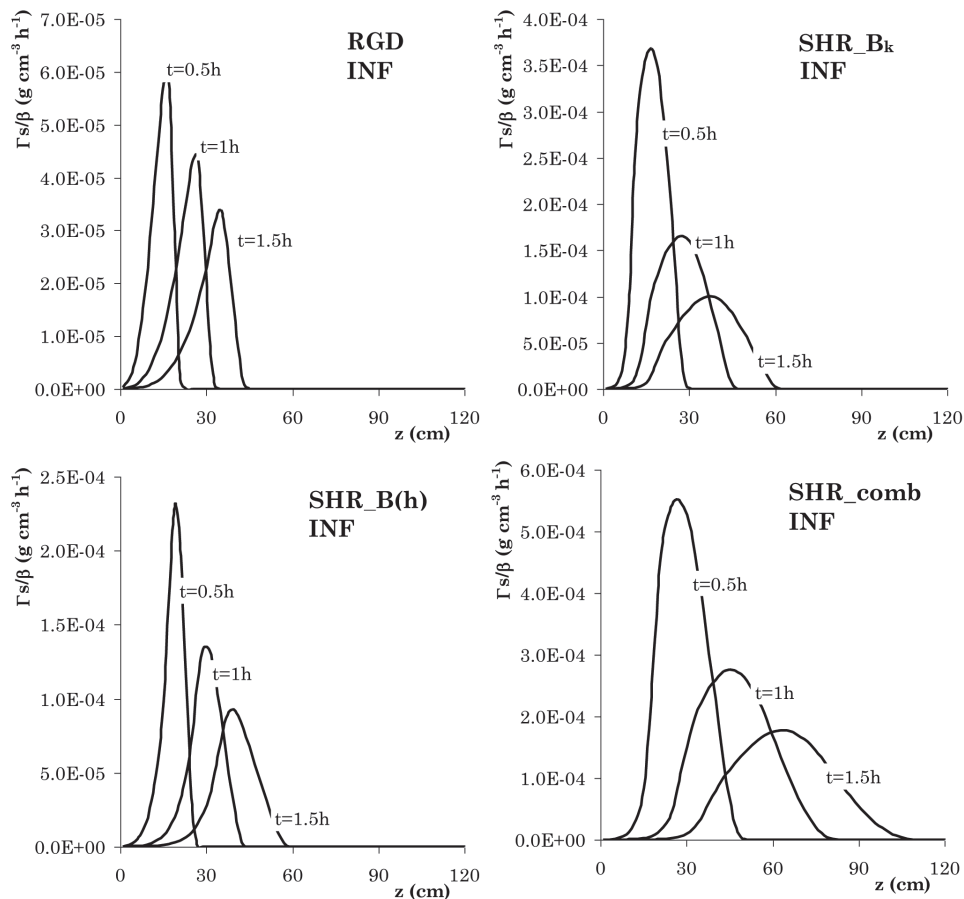


Fig. 11. Depth–time evolution of solute transfer from the fracture to the matrix domain simulated under the different scenarios for the infiltration process.

exchange term (Fig. 13) is quite uniform with depth in all the SHR scenarios, the RGD exchange term changes significantly over depth, along a depth interval increasing over time.

Water Fluxes

Finally, the graphs in Fig. 14 show the water flux densities and the cumulative fluxes at two different depths (20 and 60 cm) for both the infiltration and the drainage process simulations. These depths were selected to evaluate the hydrological behavior of the porous medium in terms of percolation fluxes, leaving a hypothetical surface root zone layer. All the curves refer to the bulk soil as they were obtained by combining the fracture and aggregate domain contributions. As for the wetting front and solute concentration propagations, the largest divergences in the fluxes were observed between scenarios RGD and SHRcomb. In general, the cumulative fluxes take approximately the same shape, but with the SHRcomb scenario yielding by far the largest amount of cumulative fluxes. This is especially true for the infiltration process. When considering the drainage process, the cumulative fluxes take on slightly different values under the different scenarios, with the largest in $\text{SHR}\beta(h)$ and SHRcomb, and the lowest under the $\text{SHR}\beta_k$ scenario.

Discussion and Conclusions

When modeling flow through fractured soils, the porous medium has previously been considered to be rigid, such that the fractures are assumed permanent and not changing with the water content. More realistic, however, is to assume the dynamic change of relative volumes of fracture and matrix domains with water contents for a shrinking soil inducing deformation of soil structure in the soil profile. We showed that taking the shrinkage curve into account may be a fundamentally important extension of dual-permeability for better understanding of water movement in soil under realistic field conditions.

As briefly mentioned in the introduction, RGD and SHR should not be seen as complementary but rather as alternative approaches. To further clarify this point, let us consider a hypothetical water flow experiment to be performed on either a large soil column or a field plot. We will assume that this can be considered as the bulk soil, including a relatively slow and a relatively fast flow domain. Sensors are placed at a depth in the soil for measuring water contents and pressure heads of the bulk soil.

Let us therefore imagine, then, that we apply water ponding to the soil surface to saturate the soil column. Thus we will let the initially saturated bulk soil gradually dry (by evaporation and/or a drainage

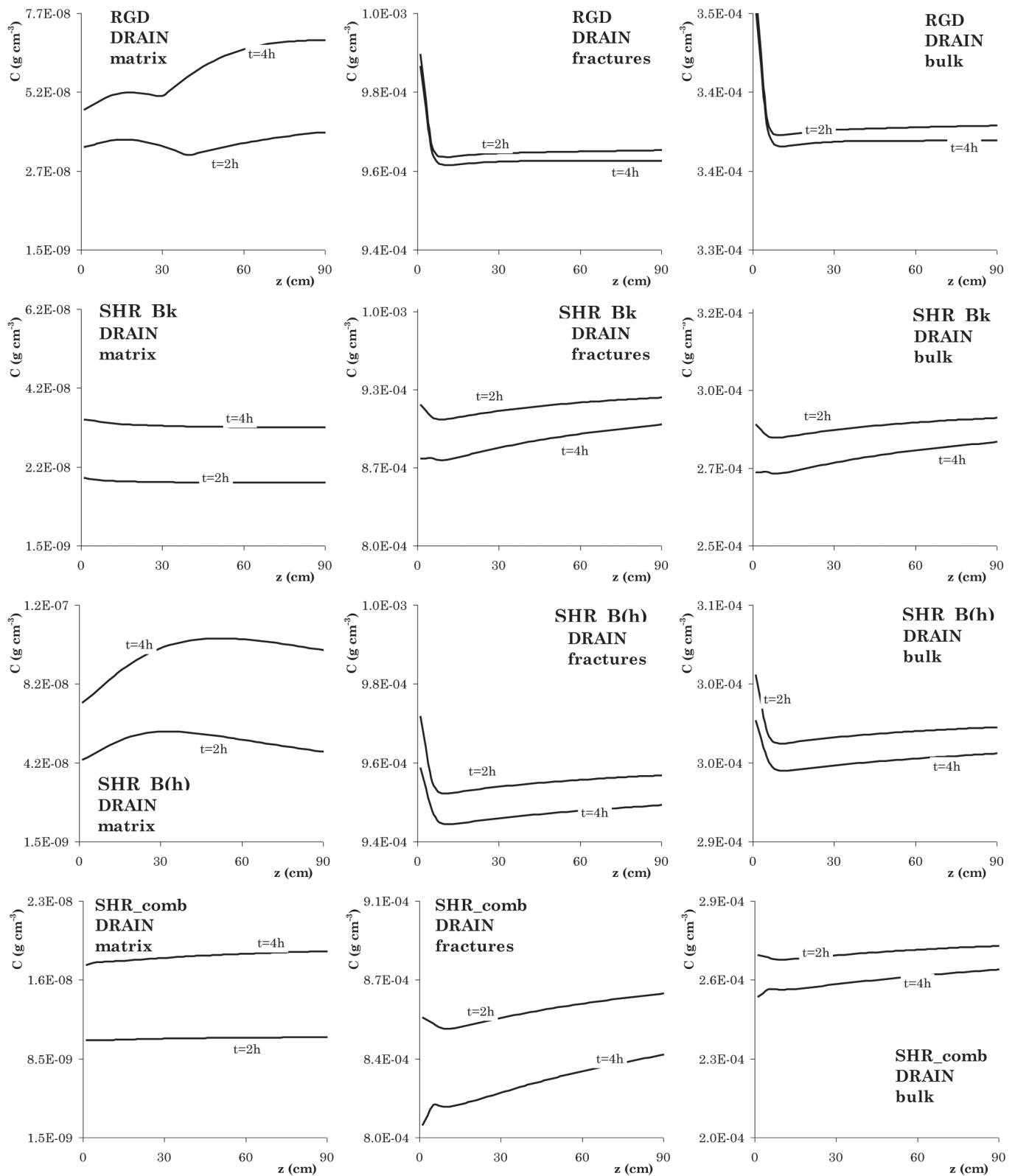


Fig. 12. Concentration profiles obtained under the different conditions, separately for the matrix and the fracture domains, for the drainage process. The graphs in the last column in the figure summarize the results of the bulk soil for all the simulation scenarios.

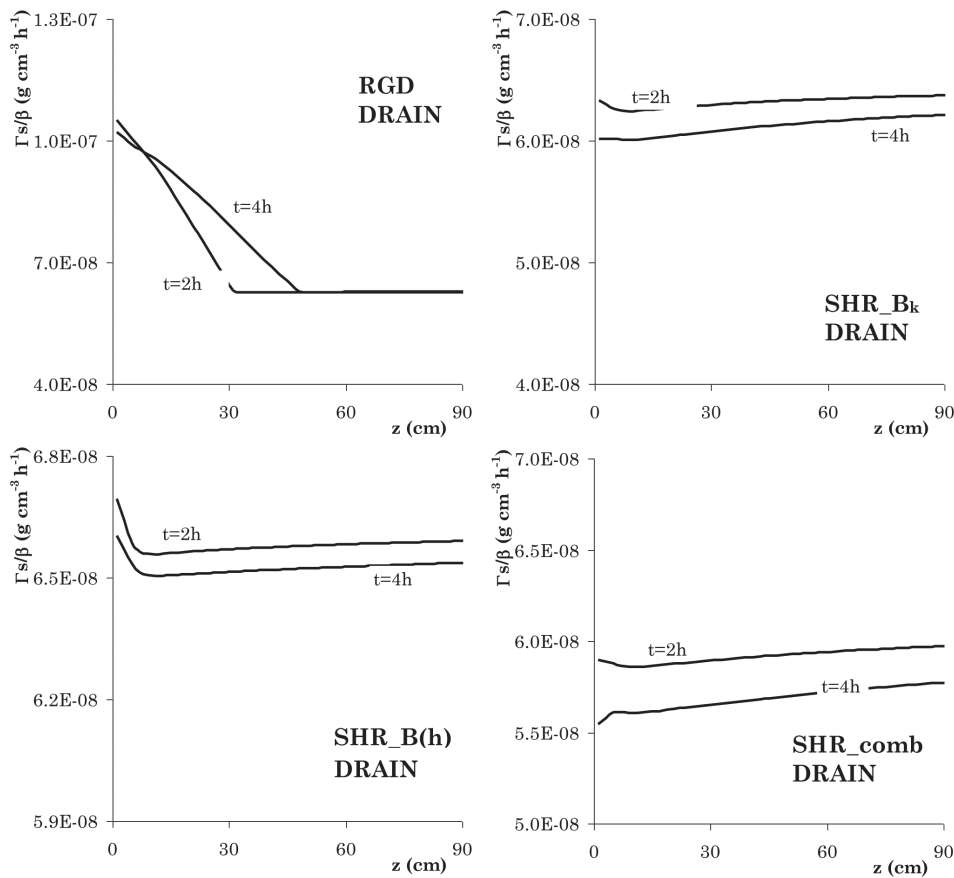


Fig. 13. Depth-time evolution of solute transfer from the fracture to the matrix domain simulated under the different scenarios for the drainage process.

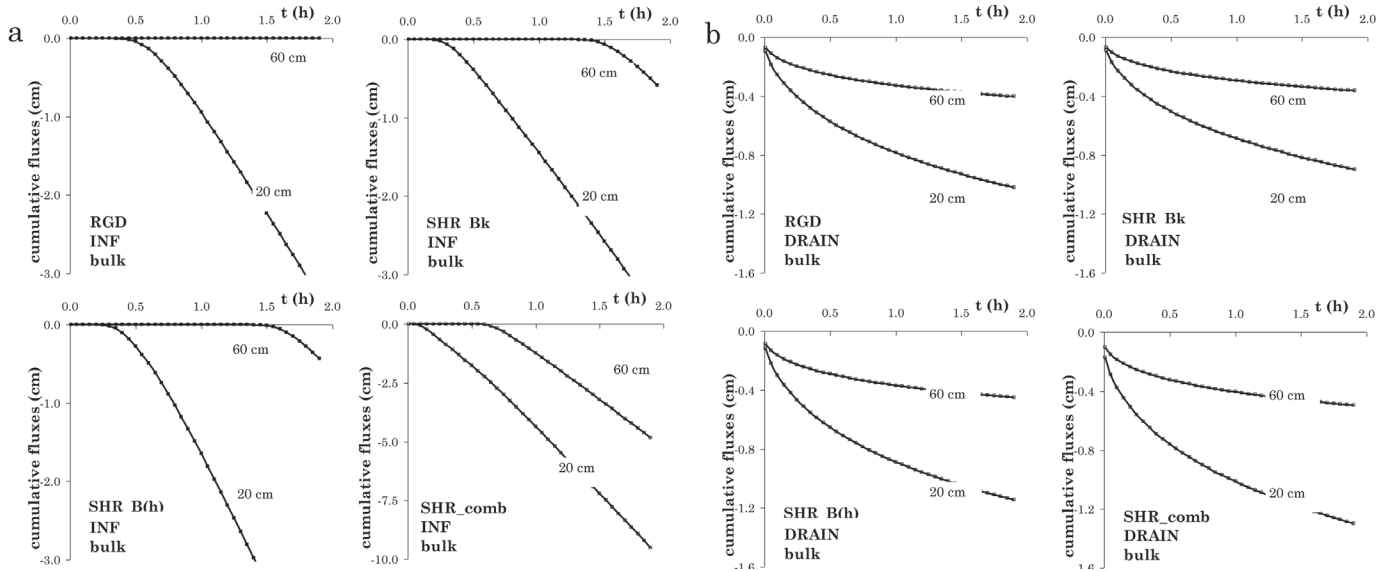


Fig. 14. Cumulative water fluxes at two different depths (20 and 60 cm). All the curves refer to the bulk soil. (a) The upper four graphs refer to the infiltration process, while (b) the lower four graphs refer to the drainage process.

process). We can monitor the evolution of the water content and the pressure head at the control depth, obtaining experimental points of the bulk water retention curve.

Now the question is: do the two domains remain rigid during drying or do they change due to a possible matrix shrinkage? In the first case, porosities and in general the geometrical

characteristics of the two domains will remain constant (not change with drying). In the second case, porosities and domain geometry (hence the two-domain hydraulic properties) will change during drying. Under the two assumptions, one could describe equally well the experimental bulk water retention curve but obtain completely different hydraulic parameters for the two domains. Obviously, such an analysis also applies to a wetting water flow process, with the matrix, which may either remain rigid or swell while wetting.

The obvious practical consequence is that, with the hydraulic properties obtained under the two assumptions, the relative contribution of the two domains to a hydrological process (infiltration, drainage, evaporation, solute transport) will differ according to the actual scenario (RGD or SHR).

In this paper, we took into account the shrinkage characteristics of the aggregate domain by considering three alternative SHR scenarios:

- Changing the hydraulic properties of both the domains and keeping the weight constant (SHR β_k)
- Fixing the aggregate and fracture hydraulic properties and allowing the weight to change with h according to the shrinkage relationship, SHR $\beta(h)$
- Changing partly the hydraulic properties and partly the weight with h (SHRcomb)

As discussed by Coppola et al. (2012), the last approach seems more physically plausible, as one might reasonably expect the aggregate shrinkage–swelling process to change the hydraulic properties of the two domains but also their relative contribution to an observed hydrological variable. As a simplifying assumption, one could also assume that this relative contribution does not change and that the shrinkage–swelling only changes the hydraulic properties of the two domains (the second SHR approach). Finally, the SHR β_k scenario was introduced here more with speculative aims, as it seems physically implausible that shrinkage–swelling dynamics changes only the contribution of the two domains, leaving the hydraulic properties unaltered, and yet this simplifying assumption may be especially useful to infer information on the shape of the $\beta(h)$ curve and to isolate its partial effects on the hydrological behavior of a shrinking dual-permeability porous medium.

Unfortunately, there is no way to establish a priori which of the three scenarios actually applies. This should be established case by case by monitoring water and/or solute fluxes at one or more control depths, which will be the main specific target of a new paper. Specifically, the decision of which modeling concept may be more appropriate to change the fractional contribution of the matrix and the fracture domain contributions to the water flow and transport behavior of the bulk soil under shrinkage may only be established on the basis of the datasets available and may also

depend on the process to be simulated. Indeed, we saw that the approaches significantly deviated during an infiltration process. By contrast, during a drying process, the water content redistribution process practically overlapped under all the hypotheses. This suggests that the sensitivity of modeling results on the different conceptual assumptions to account for shrinkage depends on the process under study and tends to decrease with water content and nonequilibrium conditions. This, in other words, suggests that a drainage process does not contain enough information to establish the most effective modeling concept to be invoked for a shrinking–swelling porous medium. For the same reasons, a drainage process does not contain enough information to estimate robustly the dual set of soil hydraulic and transport parameters.

The most important assumption of the model presented in this paper consists in the inversely proportional volume changes of the fracture and matrix domains during the swell–shrink dynamics, which, in turn, affect the mass transfer, while the overall porosity of the bulk soil, and hence the layer thickness, remains constant. This implies a dominant cracking over subsidence, such that the swell–shrink behavior of soil aggregates may be mostly accommodated within a crack network. In any case, we believe that the model might be universally applied for field-scale applications. To us, the approximation of overlooking subsidence phenomena may well lie within the uncertainties related to the difficulties of determining independently the dual set of soil hydraulic and transport parameters, the water and solute transfer parameters characterizing the soil matrix–fracture interface, and, even worse, their spatial variability. In any case, it may be included in later development stages of the model.

Finally, including the effect of hysteresis in soil deformation during shrinking–swelling cycles is expected to further improve the prediction strength of the approach for shrinking soils under dominant cracking conditions.

Acknowledgments

The authors are grateful to Fabio Mura for providing the image in Fig. 1 of this paper. We also acknowledge the very helpful comments of the referees.

Appendix

Dual-Permeability Model for Soil Water Flow and Solute Transport

According to the dual-permeability formulation proposed by Gerke and van Genuchten, (1993a), the following two coupled mixed-type Richards equations may be used to describe the vertical one-dimensional transient water flow in fracture domain (Eq. [A1a]) and the pore region of the aggregates (Eq. [A1b]) (subscript f for fracture domain and subscript a for aggregate domain):

$$C_{p_f}(h_f) \frac{\partial h_f}{\partial t} = \frac{\partial}{\partial z} \left(K_f \frac{\partial h_f}{\partial z} - K_f \right) - \frac{\Gamma_w}{\beta_f} - S_f(h_f) \quad [A1a]$$

$$Cp_a(h_a) \frac{\partial h_a}{\partial t} = \frac{\partial}{\partial z} \left(K_a \frac{\partial h_a}{\partial z} - K_a \right) + \frac{\Gamma_w}{1-\beta_f} - S_a(h_a) \quad [A1b]$$

where the flow is considered positive downward. $Cp = d\theta/dh$ (L^{-1}) is the water capacity, S (T^{-1}) the root water uptake rate, K ($L T^{-1}$) the hydraulic conductivity, and θ and h the volumetric water content and the pressure head (L), respectively. The weight β_f is the fraction of total soil occupied by the fracture pore-system ($0 < \beta_f < 1$).

Gerke and van Genuchten (1993b) described the water transfer term Γ_w (T^{-1}) as a first-order kinetic process. It is assumed to depend on the difference between the pressure heads in the two domains and is given by:

$$\Gamma_w = \alpha_w (h_f - h_a) \quad [A2]$$

α_w is a first-order mass transfer coefficient ($L^{-1} T^{-1}$) and may be calculated as

$$\alpha_w = \frac{\eta}{l^2} K_{af} \gamma_w \quad [A3]$$

where K_{af} is the effective hydraulic conductivity function of the fracture–aggregate systems interface evaluated here in terms of both h_f and h_a as:

$$K_{af} = 0.5 [K_{af}(h_f) + K_{af}(h_a)] \quad [A4]$$

In Eq. [A3], η is a dimensionless geometry-dependent coefficient (Gerke and van Genuchten, 1996), l is a characteristic length of the matrix structure, and γ_w is a dimensionless scaling coefficient for which a value of 0.4 was suggested (Gerke and van Genuchten, 1993b).

Similar to Eq. [A1], solute transport in a dual-permeability porous system is governed by two coupled advection–dispersion equations as follows

$$\frac{\partial \theta_f C_f}{\partial t} = \frac{\partial}{\partial z} \left(\theta_f D_f \frac{\partial C_f}{\partial z} \right) - \frac{\partial q_f C_f}{\partial z} - \frac{\Gamma_s}{\beta_f} \quad [A5a]$$

$$\frac{\partial \theta_a C_a}{\partial t} = \frac{\partial}{\partial z} \left(\theta_a D_a \frac{\partial C_a}{\partial z} \right) - \frac{\partial q_a C_a}{\partial z} - \frac{\Gamma_s}{1-\beta_f} \quad [A5b]$$

where C is the solute concentration ($L^3 M^{-1}$), q is the volumetric flux density ($L T^{-1}$), D is the dispersion coefficient ($L^2 T^{-1}$), and Γ_s is the solute mass transfer term ($M L^{-3} T^{-1}$) evaluated as the sum of diffusive and advective fluxes:

$$\Gamma_s = \alpha_s (1-\beta_f) (C_f - C_a) + \Gamma_w C^* \quad [A6]$$

where α_s is a first-order diffusive solute mass transfer coefficient (T^{-1}), and C^* is equal to C_f for $\Gamma_w > 0$ and C_a for $\Gamma_w < 0$.

The dispersion coefficient is generally assumed to be of the form:

$$D = D_0 \tau + \lambda v \quad [A7]$$

where D_0 ($L^2 T^{-1}$) is the molecular diffusion coefficient, λ the dispersivity, v the average pore water velocity ($v = q/\theta$), q the Darcian flux, and τ a tortuosity factor ($\tau = \theta^{7/3}/\theta_0$), with θ_0 the water content for $h = 0$ (Millington and Quirk, 1961).

The first-order mass transfer coefficient has the form:

$$\alpha_s = \frac{\eta}{l^2} D_i \quad [A8]$$

where η and l are the same as for water and D_i is the effective diffusion coefficient of the soil matrix at the fracture–matrix interface.

Parametric Functions for Shrinkage Curves

The fitting approximations of the shrinkage curve remain especially useful for numerical applications. Indeed, the shrinkage curve is frequently described by using continuous functions (Braudeau et al., 1999; Groenevelt and Grant, 2001; Peng and Horn, 2005; Peng et al., 2005; Boivin et al., 2006a,b).

The equation proposed by Peng and Horn (2005) for $e_a(\vartheta_a)$:

$$e_a(\vartheta_a) = e_{r,a} + \frac{e_{0,a} - e_{r,a}}{\left[1 + \left(\frac{\alpha_{c,a} \vartheta_a}{e_{0,a} - \vartheta_a} \right)^{-n_{c,a}} \right]^{m_{c,a}}} \quad [A9]$$

corresponds to an S-shaped sigmoid curve. Similarly, $e_a(h_a)$ can also be described by an S-shaped sigmoid curve resembling van Genuchten's equation for water retention (van Genuchten, 1980):

$$e_a(h_a) = e_{r,a} + \frac{e_{0,a} - e_{r,a}}{\left[1 + \left(\alpha_{c,a}^* |h_a| \right)^{n_{c,a}^*} \right]^{m_{c,a}^*}} \quad [A10]$$

In both equations, α_c , n_c , and m_c are shape parameters. The asterisk indicates that the parameters in Eq. [4] differ from those in Eq. [3]. Parameters e_0 and e_r are the saturated and residual void ratio corresponding to saturated $\vartheta_{0,a}$ (at $h_a = 0$) and residual $\vartheta_{r,a}$ (for $h_a \rightarrow -\infty$), respectively.

References

- Abou Najm, M.R., J. Jabro, W.M. Iversen, R.H. Mohtar, and R.G. Evans. 2010. New method for the characterization of three-dimensional preferential flow paths in the field. *Water Resour. Res.* 46. doi:10.1029/2009WR008594
- Beven, K., and P. Germann. 1982. Macropores and water flow in soils. *Water Resour. Res.* 18:1311–1325. doi:10.1029/WR018i005p01311
- Boivin, P., P. Garnier, and M. Vauclin. 2006a. Modeling the soil shrinkage and water retention curves with the same equations. *Soil Sci. Soc. Am. J.* 70: 1082–1093. doi:10.2136/sssaj2005.0218
- Boivin, P., B. Schaeffer, E. Temgoua, M. Gratiot, and G. Steinman. 2006b. Assessment of soil compaction using soil shrinkage modelling: Experimental data and perspectives. *Soil Tillage Res.* 88:65–79. doi:10.1016/j.still.2005.04.008
- Braudeau, E., J.M. Costantini, G. Bellier, and H. Colleuille. 1999. New device and method for soil shrinkage curve measurement and characterization. *Soil Sci. Soc. Am. J.* 63:525–535. doi:10.2136/sssaj1999.03615995006300030015x
- Bronswijk, J.J.B. 1991. Relation between vertical soil movements and water-content changes in cracking clays. *Soil Sci. Soc. Am. J.* 55:1220–1226. doi:10.2136/sssaj1991.03615995005500050004x
- Bruand, A., H. Cohcrane, P. Fisher, and R.J. Gilkes. 2001. Increase in the bulk density of a Grey Clay subsoil by infillings of cracks by topsoil. *Eur. J. Soil Sci.* 52:37–47. doi:10.1046/j.1365-2389.2001.t01-1-00365.x
- Castiglione, P., B.P. Mohanty, P.J. Shouse, J. Šimůnek, M.Th. van Genuchten, and A. Santini. 2003. Lateral water diffusion in an artificial macroporous system: Modeling and experimental evidence. *Vadose Zone J.* 2:212–221. doi:10.2136/vzj2003.2120
- Chertkov, V.Y. 2007a. The soil reference shrinkage curve. *Open Hydrol. J.* 1:1–18. doi:10.2174/1874378100701010001
- Chertkov, V.Y. 2007b. The reference shrinkage curve at higher than critical soil clay content. *Soil Sci. Soc. Am. J.* 71(3):641–655. doi:10.2136/sssaj2006.0146
- Chertkov, V.Y. 2008. Estimating the aggregate/intraaggregate mass ratio of a shrinking soil. *Open Hydrol. J.* 2:7–14. doi:10.2174/1874378100802010007
- Coppola, A., G. Dragonetti, A. Comegna, P. Zdruli, N. Lamaddalena, S. Pace, and L. De Simone. 2014. Mapping solute deep percolation fluxes at regional scale by integrating a process-based vadose zone model in a Monte Carlo approach. *Soil Sci. Plant Nutr.* doi:10.1080/00380768.2013.855615.
- Coppola, A., H. H. Gerke, A. Comegna, A. Basile, and V. Comegna. 2012. Dual-permeability model for flow in shrinking soil with dominant horizontal deformation. *Water Resour. Res.* 48:8. doi:10.1029/2011WR011376.
- Coppola, A., V. Comegna, A. Basile, N. Lamaddalena, and G. Severino. 2009b. Darcian preferential water flow and solute transport through bimodal porous systems: Experiments and modeling. *J. Contam. Hydrol.* doi:10.1016/j.jconhyd.2009.10.004.
- Coppola, A., M. Kutilek, and E.O. Frind. 2009a. Transport in preferential flow domains of the soil porous system: Measurement, interpretation, modelling, and upscaling. *J. Contam. Hydrol.* doi:10.1016/j.jconhyd.2008.05.011.
- Coppola, A., and L. Randazzo. 2006. A Matlab code for the transport of water and solutes in unsaturated soils with vegetation. Tech. Rep. Soil and Contaminant Hydrology Lab., DITEC, University of Basilicata, Potenza, Italy.
- Dušek J., T. Vogel, L. Lichner, A. Čipáková, and M. Dohnal. 2006. Simulated cadmium transport in macroporous soil during heavy rainstorm using dual-permeability approach. *Biologia 61/Suppl.* 19:251–254
- Emmerman, S.H. 1995. The tipping bucket equations as a model for macropore flow. *J. Hydrol.* 171:23–47. doi:10.1016/0022-1694(95)02735-8
- Garnier, P., M. Rieu, P. Boivin, M. Vauclin, and P. Baveye. 1997. Determining the hydraulic properties of a swelling soil from a transient evaporation experiment. *Soil Sci. Soc. Am. J.* 61:1555–1563. doi:10.2136/sssaj1997.03615995006100060003x
- Gerke, H.H., and J.M. Köhne. 2004. Dual-permeability modeling of preferential bromide leaching from a tile-drained glacial till agricultural field. *J. Hydrol.* 289:239–257. doi:10.1016/j.jhydrol.2003.11.019
- Gerke, H.H., and M.Th. van Genuchten. 1993a. A dual porosity model for simulating the preferential movement of water and solute in structured porous media. *Water Resour. Res.* 29:305–319. doi:10.1029/92WR02339
- Gerke, H.H., and M.Th. van Genuchten. 1993b. Evaluation of a first-order water transfer term for variably saturated dual-porosity flow models. *Water Resour. Res.* 29:1225–1238. doi:10.1029/92WR02467
- Gerke, H.H., and M.Th. van Genuchten. 1996. Macroscopic representation of structural geometry for simulating water and solute movement in dual-porosity media. *Adv. Water Resour.* 19:343–357. doi:10.1016/0309-1708(96)00012-7
- Germann, P., and K. Beven. 1985. Kinematic wave approximation to infiltration into soils with sorbing macropores. *Water Resour. Res.* 21(7):990–996. doi:10.1029/WR021i007p00990
- Greco, R. 2002. Preferential flow in macroporous swelling soil with internal catchment: Model development and applications. *J. Hydrol.* 269(3-4):150–168. doi:10.1016/S0022-1694(02)00215-9
- Groenevelt, P.H., and C.D. Grant. 2001. Re-evaluation of the structural properties of some British swelling soils. *Eur. J. Soil Sci.* 52:469–477. doi:10.1046/j.1365-2389.2001.00388.x
- Hoogmoed, W.B., and J. Bouma. 1980. A simulation model for predicting infiltration into cracked clay soil. *Soil Sci. Soc. Am. J.* 44:458–461. doi:10.2136/sssaj1980.03615995004400030003x
- Horn, R. 2004. Time dependence of soil mechanical properties and pore functions for arable soils. *Soil Sci. Soc. Am. J.* 68(4):1131–1137. doi:10.2136/sssaj2004.1131
- Jarvis, N.J. 2007. Review of non-equilibrium water flow and solute transport in soil macropores: Principles, controlling factors and consequences for water quality. *Eur. J. Soil Sci.* 58:523–546. doi:10.1111/j.1365-2389.2007.00915.x
- Jarvis, N.J. 1994. The MACRO model (version 3.1) Technical description and sample simulations. Reports and Dissertations no. 19. Swedish Univ. of Agricultural Sciences, Dep. of Soil Sciences, Uppsala.
- Klute, A., and C. Dirksen. 1986. Hydraulic conductivity and diffusivity: Laboratory methods. In: A. Klute, editor, *Methods of soil analysis. Part 1. Physical and mineralogical methods.* Agron. Monogr. 9, 2nd ed. SSSA and ASA, Madison, WI. p. 687–734. doi:10.2136/sssabookser5.1.2ed.c28
- Larsbo, M., and N.J. Jarvis. 2003. MACRO5.0. A model of water flow and solute transport in macroporous soil. Technical description. Studies in the Biogeophysical Environment, Emergo 2003:6. Dep. of Soil Sciences, SLU, Uppsala, Sweden.
- Millington, R.J., and J.M. Quirk. 1961. Permeability of porous solids. *Trans. Faraday Soc.* 57:1200–1207. doi:10.1039/HF9615701200
- Mualem, Y. 1976. A new model for predicting the hydraulic conductivity of unsaturated porous media. *Water Resour. Res.* 12:513–522. doi:10.1029/WR012i003p00513
- Peng, X., and R. Horn. 2005. Modeling soil shrinkage curve across a wide range of soil types. *Soil Sci. Soc. Am. J.* 69:584–592. doi:10.2136/sssaj2004.0146
- Peng, X., and R. Horn. 2007. Anisotropic shrinkage and swelling of some organic and inorganic soils. *Eur. J. Soil Sci.* 58:98–107. doi:10.1111/j.1365-2389.2006.00808.x
- Peng, X., R. Horn, D. Deery, M.B. Kirkham, and J. Blackwell. 2005. Influence of soil structure on the shrinkage behaviour of a soil irrigated with saline-sodic water. *Aust. J. Soil Res.* 43:555–563. doi:10.1071/SR04116
- Peters, R.R., and E.A. Klavetter. 1988. A continuum model for water movement in an unsaturated fractured rock mass. *Water Resour. Res.* 24:416–430. doi:10.1029/WR024i003p00416
- Ray, C., T. Vogel, and J. Dušek. 2004. Modeling depth-variant and domain-specific sorption and biodegradation in dual-permeability media. *J. Contam. Hydrol.* 70:63–87. doi:10.1016/j.jconhyd.2003.08.009
- Richards, B.G., and S. Peth. 2009. Modelling soil physical behaviour with particular reference to soil science. *Soil Tillage Res.* 102(2):216–224. doi:10.1016/j.still.2008.07.022
- Steenhuis, T.S., J.Y. Parlange, and M.S. Andreini. 1990. A numerical model for preferential solute movement in structured soils. *Geoderma* 46:193–208. doi:10.1016/0016-7061(90)90015-2
- Tuller, M., and D. Or. 2003. Hydraulic functions for swelling soils: Pore scale considerations. *J. Hydrol.* 272:50–71. doi:10.1016/S0022-1694(02)00254-8
- van Genuchten, M.Th. 1980. A closed-form equation for predicting the hydraulic conductivity of unsaturated soils. *Soil Sci. Soc. Am. J.* 44:892–898. doi:10.2136/sssaj1980.03615995004400050002x
- Wallach, R., T.S. Steenhuis, and J.Y. Parlange. 1998. Modeling the movement of water and solute through preferential flow paths. In: J. Delleur, editor, *The handbook of groundwater engineering.* CRC Press, Boca Raton, FL. p. 7-1–7-21.
- Wind, G.P. 1968. Capillary conductivity data estimated by simple method. In: P.E. Rijtema and H. Wassink, editors, *Water in the unsaturated zone. Proc. of the Wageningen Symp., Vol. 1.* Int. Assoc. of Hydrol. Sci., Gentbrugge, Belgium. p. 181–191.